TWO NOVEL STAINING METHODS FOR COMBINED FUNCTIONAL AND STRUCTURAL ANALYSIS OF SINGLE CNS SYNAPSES

by

HOSSEIN SHAYAN

B.Sc. (Hon), University of British Columbia, 1995

A THESIS SUBMITTED IN PARTIAL FULFILLMENT OF THE REQUIREMENT

FOR THE DEGREE OF

Master of Science

in

THE FACULTY OF GRADUATE STUDIES

Graduate program in neuroscience

We accept this thesis as conforming

to the required standard

THE UNIVERSITY OF BRITISH COLUMBIA

August 1998

© Hossein Shayan, 1998

In presenting this thesis in partial fulfilment of the requirements for an advanced degree at the University of British Columbia, I agree that the Library shall make it freely available for reference and study. I further agree that permission for extensive copying of this thesis for scholarly purposes may be granted by the head of my department or by his or her representatives. It is understood that copying or publication of this thesis for financial gain shall not be allowed without my written permission.

Department of Psychiatry

The University of British Columbia
Vancouver, Canada

Date August 19/98

ABSTRACT

The great diversity in morphology, receptor composition, and vesicle content of CNS synapses suggests that structural changes are important events in the establishment of neuronal plasticity. We have developed two novel methods for conducting functional/structural correlation studies of single CNS synapses. In the first method, a neuron is filled with biocytin and fluo-3 (a Ca^{2+} indicator), imaged with a CCD camera for changes in $[Ca^{2+}]_i$, reacted with fluorescein-conjugated avidin and imaged by confocal microscopy. Imaging of the $[Ca^{2+}]_i$ allows for the functional assessment of a single synapse, and confocal microscopy allows for the measurement of the spine size and its reconstruction in 3D. To permit electron microscopic examination of the same synapse, the cell is reacted with biotinylated anti-avidin antibody and is visualized by a commercially available ABC kit. This technique allows the examination of the structure of a functionally characterized synapse at both light and electron microscopic levels.

While physiological imaging methods permit the resolution of activity of single presynaptic and postsynaptic elements, it has not been possible to unequivocally examine the array of proteins expressed at these same structures. This problem arises from the inability of current immunocytochemical techniques to differentiate between a process of the neuron of interest and the surrounding neuropil belonging to other cells. Thus, with our second method, we have sought to develop an antibody staining technique which would restrict reactivity to only a single neuron. Our assay involves preloading a single neuron with the coupling reagent biocytin. Following fixation, the injected biocytin is then complexed with avidin-linked glucose oxidase providing a means of locally generating hydrogen peroxide within a cell of interest which catalyzes the peroxidase-mediated (coupled to primary antibody) staining reaction. We have used this method successfully with antibodies to a number of neuronal markers (neuron-specific enolase, neurofilament, microtubule-associated protein, and AMPA receptor GluR 2/3). Our staining method enables subcellular resolution of immunocytochemical markers within a single neuron without confounding staining of neighboring cells. We anticipate that these two approaches will facilitate the study of neuronal phenotype in fine dendritic processes in electrophysiologically characterized neurons in specimens with a complex neuropil such as brain slices or high density cultures.

TABLE OF CONTENTS

Abstract ii

Table of Contents iv

List of Tables vii

List of Figures viii

List of Abbreviations ix

Acknowledgements xi

CHAPTER I Introduction 1

- 1.1 Historical Perspective 1
- 1.2 Synaptic strength and information storage 1
- 1.3 Synaptic structure as a determinant of synaptic strength 3
- 1.4 Current methods of structural analysis 4
- 1.5 Current methods of functional analysis 6
  - 1.5.1 Electrophysiology 6
  - 1.5.2 Imaging 8
    - 1.5.2.1 Fluorescent indicators 9
    - 1.5.2.2 Imaging techniques 10
- 1.6 Research Hypothesis 12

CHAPTER II Materials and Methods 14

- 2.1 Cell Culture 14

2.2 Intracellular calcium imaging and analysis 14

2.3 Confocal Microscopy and Analysis 15

2.4 Electron microscopy 16

2.5 Assay of GO distribution 17

2.6 Immunofluorescent staining of neuron-specific enolase 18

2.7 Single cell staining 18

2.8 Conjugation of catalase beads 19

CHAPTER III A 3 step approach to correlative functional and structural analysis of single CNS synapses 21

3.1 Resolution of wide-field microscopy versus confocal microscopy 21

3.2 Correlative functional and structural analysis 24

CHAPTER IV Restriction of peroxidase-mediated antibody reactivity to single neurons by local H_2O_2 production 29

4.1 Local generation of H_20_2 by glucose oxidase 29

4.2 Optimal duration of GO incubation 29

4.3 Effect of fixative on GO distribution 32

4.4 Fluorescence double labeling lacks resolution of DAB mediated single staining 35

4.5 Staining of single neurons for antibody reactivity 35

4.6 Specificity of single cell method at the ultrastructural level 38

4.7 Detection of single quantal synaptic responses and AMPA -type glutamate receptor subunits at single synapses 41

4.8 Peroxide clearance of catalase conjugated beads 47

CHAPTER V Discussion 53

5.1 A combined method for functional and structural examination of a single synapse 53

5.2 Local generation of H_2O_2 by glucose oxidase allows for restriction of antibody staining to a single cell 56

5.3 Penetration properties of avidin compared to that of avidin conjugated to glucose oxidase 57

5.4 Glutaraldehyde prevents the penetration of avidin conjugated to glucose oxidase into cells 57

5.5 Distribution of NSE within a single cortical neuron 58

5.6 Specificity of single cell method at the ultrastructural level as revealed by GluR 2/3 staining 59

5.7 Localization of AMPA-type glutamate receptors at functionally characterized synapses 60

5.8 Future considerations for the application of single-cell staining 61

5.9 Conclusions 62

Literature Cited 63

LIST OF TABLES

Table 1. Heterogeneity in spine sizes of functionally characterized synapses 28

LIST OF FIGURES

Figure-1. Measurement of the lateral resolution of the wide-field and confocal microscopy. 23

Figure-2. Correlative functional and structural examination of single CNS synapses. 26

Figure-3. Schematic representation of single cell staining. 31

Figure-4. The distribution of glucose oxidase-dependent staining within a cell is dependent on the fixation method. 34

Figure-5. Localization of neuron-specific enolase using immunofluorescence double labeling. 37

Figure-6. Localization of neuron-specific enolase using single cell staining. 40

Figure-7. Specificity of single cell staining demonstrated using electron microscopy. 43

Figure-8. Localization of GluR 2/3 subunits at functionally characterized synapses. 46

Figure-9. Localization of GluR 2/3 subunits at single CNS synapses. 49

Figure-10. Peroxide clearance activity of catalase-conjugated agarose. 52

LIST OF ABBREVIATIONS

Ab	Antibody
ABC	Avidin-biotin complex
AMPA	α-amino-3-hydroxy-5-methyl-4-isoxazolepropionic acid
Av-GO	Avidin conjugated to glucose oxidase
Ca^{2+}	Calcium
CCD	Charge-coupled devices
CLSM	Confocal laser scanning microscopy
CNS	Central nervous system
DAB	Diaminobenzidine
EM	electron microscopy
GluR	Glutamate receptor
gm	gram
GO	Glucose oxidase
HRP	Horseradish peroxidase
K^+	Potassium
Kd	Dissociation constant
KDa	kilodalton
kV	kilovolts
LTD	Long-term depression
LTP	Long-term potentiation

M	molar
MB	megabytes
Mg^{2+}	Magnesium
μg	microgram
μM	micromolar
ml	milliliter
mm	millimeter
mM	millimolar
ms	millisecond
min	Minute
MSCT	Miniature synaptic calcium transient
Ni	Nickel
nm	nanometer
NMDA	N-methyl-D-aspartate
NSE	Neuron-specific enolase
PBS	Phosphate-buffered saline
PMT	Photomultiplier tube
PSD	Postsynaptic density
SD	Standard deviation
TPLSM	Two photon laser scanning microscopy
TTX	Tetrodotoxin
vol.	Volume

ACKNOWLEDGEMENTS

I am grateful to Dr. T. Murphy for his support and guidance as my supervisor. A very special thanks goes to Paul Mackenzie without whom I would not have been able to realize this thesis. Thanks to Gail Kenner, as well as O. Prange, Dr. H. Nakazawa, D. Ho, A. So, Dr. S. Duffy, and A. Moshaver for their help and more importantly for making this an enjoyable experience. Thanks to my great friend Fred Chen for proofreading this thesis. Further thanks go to my committee members Dr. P. Reiner, Dr. T. O' Connor, and Dr. W. Tetzlaff for their guidance and suggestions. Finally, I would like to thank my parents, my brother, and all my friends for their endless support and love.

CHAPTER I

Introduction

1.1 Historical perspective

Understanding the underlying cellular mechanisms involved in learning and memory formation has intrigued neurobiologists for decades. Integration of information at various levels ranging from changes in neuronal circuitry to changes in discrete synaptic molecules have been implicated as fundamental events in memory formation and storage. More recently, the consensus has shifted toward the idea that the patterns of synaptic strength provide the most basic level of information integration for memory storage (Stevens and Sullivan, 1998; Stevens, 1996). To date, no direct evidence in support of this idea exists, however with the development of new techniques in the past decade, a flurry of experimental reports have emerged to describe how synaptic strength is altered by experience and therefore how memories might be stored.

1.2 Synaptic strength and information storage

The generation of an action potential in a presynaptic neuron eventually leads to the release of neurotransmitter into the synaptic cleft. Binding of neurotransmitter to specific receptors on the membrane of the postsynaptic neuron results in a brief, highly localized, voltage change (the postsynaptic potential), the average amplitude of which is a measure of the strength of that synapse. The idea that the strength as well as the number of synapses could be altered in response to experience was first postulated by Ramon y Cajal (1911) and further developed by Hebb (1949) and Eccles (1965). In principle, the fact that a typical CNS neuron such as a hippocampal neuron from the CA1 region has 23800 ± 7100 synapses (Bannister and Larkman, 1995) allows a single neuron to store many bits of information by simply modifying individual synapses. Indeed, there have been many reports of alterations in shapes and sizes of synapses (which in turn may influence their strength) in CNS tissue from animals trained to varying degrees or exposed to environments of different complexity (for a review see Globus, 1975; Greenough and Bailey, 1988; Bailey and Kandel, 1993; Horner, 1993; Harris and Kater, 1994).

The most widely studied cellular model of learning is by far the phenomenon of long-term potentiation (LTP). LTP refers to an apparent increase in the synaptic strength of an individual synapse (lasting for days or even weeks) in response to repeated stimulation applied in a specific manner (Bliss and Lomo, 1973; Bliss and Collingridge, 1993; Collingridge and Bliss, 1995; Kullmann and Siegelbaum, 1995). More recently, another type of synaptic modification known as long-term depression (LTD) has also been implicated as the molecular basis of information storage (Bear and Malenka, 1994). LTD refers to the long-lasting decrease in the synaptic strength induced by repeated stimulation of the same synapse.

Despite the countless number of studies undertaken, many questions still remain unanswered regarding the exact role of LTP and LTD as the building blocks of memory. These two phenomena are merely introduced to highlight the fact that studying alterations in the synaptic strength and synaptic plasticity are essential steps towards understanding higher cortical functions.

1.3 Synaptic structure as a determinant of synaptic strength

Synaptic strength can be modified in many ways. In theory, the strength of a single synapse can be increased by increasing the probability of synaptic vesicle release, increasing the number of vesicles released, increasing the neurotransmitter content of each vesicle, altering the number or type of postsynaptic receptors, or increasing the response of individual receptors. These changes in turn, can result from several different processes such as phosphorylation or dephosphorylation of receptors, or by altering the structure of the pre- or postsynaptic compartments. For instance, the activity of various receptors including N-methyl-D-aspartate (NMDA) receptors (a subclass of ionotropic glutamate receptors implicated in both LTP and LTD) can be altered by phosphorylating various sites on the receptor (Raymond et al., 1993). Indeed, many models have postulated that activity-dependent upregulation of specific kinases and phosphatases is essential to the maintenance of LTP and LTD (Lisman, 1989). However, the great diversity in shapes, receptor composition, and vesicle content of CNS synapses has also focused the attention on structural changes as an important event in stabilizing neuronal plasticity. Numerous reports have already demonstrated the role of synaptic morphology and structure in formulating responses to various training paradigms in invertebrates (Wojtowicz et al., 1994). While the complexity of the vertebrate CNS has impeded the discovery of similar findings, there has been evidence of changes in synaptic structure of vertebrate CNS in response to a variety of experimental protocols such as LTP and spatial learning (Hosokawa et al., 1995; Moser et al., 1994; Wallace et al., 1991; Desmond and Levy, 1988). Currently, changes in the synaptic structure have been generally accepted as the underlying basis of synaptic plasticity; however, the locus of these changes (preversus postsynaptic) remains the source of much heated debate. The main reason for the lack of any conclusive evidence is the inherent difficulty of experiments and the inability to pinpoint neuronal responses to single synapses. Ideally, in order to directly demonstrate the occurrence of structural changes in response to a physiological stimulus, one needs to simultaneously examine the structure and function of a single synapse both prior and after the application of a stimulus. In the following sections, the current experimental approaches in examining the structure and function of a single synapse will be introduced.

1.4 Current methods of structural analysis

Greater than 90% of CNS excitatory neurons synapse onto tiny dendritic protrusions known as spines (Harris and Kater, 1994). It is postulated that the dendritic spines provide morphologically and biochemically isolated environments for the regulation of individual synaptic activities (Yuste and Denk, 1995). Some of the structural features of a synapse that have been implicated in plastic changes such as LTP include the size of the spine head and neck, the number of presynaptic vesicles, the size of the postsynaptic density (PSD), the receptor composition of the PSD, and the number of the active zones per synaptic bouton. The main techniques used in examining these features include immunocytochemistry, electron microscopy (EM), and more recently confocal microscopy. Due to the small dimensions of a synapse, EM (the highest resolution technique) is by far the most popular method of examination. EM in conjunction with immunocytochemistry (for a detailed review of immunocytochemical techniques see Cuello, 1993) allows for the localization of various receptors, such as the

NMDA receptors (Huntley et al., 1994), within the postsynaptic membrane. In addition, electron microscopic examination of unlabelled synapses has been used to determine the size of dendritic spines (Sorra and Harris, 1993), the number of presynaptic vesicles (Harris and Sultan, 1995; Schikorski and Stevens, 1997), and the size of the postsynaptic density (Harris and Stevens 1989, Sorra and Harris 1993).

In the past decade, the development of confocal laser scanning microscopy (CLSM) has provided an alternative method of high spatial resolution measurement of biological structures. In CLSM, the excitation light from the source (laser) is focused on a small volume of the specimen, and the emitted light from this small volume is detected by a photomultiplier (Pawley, 1995). In a photomultiplier, incoming photons result in the ejection of secondary electrons from the photocathode. The output signal is generated by counting the number of secondary electrons ejected, in response to the intensity of each pixel within the object plane (Inoué, 1986). The term confocal refers to the fact that both the source and the exit pinholes are located confocally with respect to the illuminated section of the specimen. As a result, emission light from out of focus planes is eliminated, yielding a particularly useful technique for examining small structures buried in thick tissue sections, e.g. dendritic spines within a brain slice. By scanning the focused laser beam over a specimen an image is obtained. Optical sections of the specimen over a sequence of focal planes can be imaged using a computer driven focus motor (Schild, 1996). In contrast to EM, CLSM cannot provide information regarding the ultrastructure of a synapse; however, it still remains a powerful technique in structural examination for two reasons. Firstly, the scanning ability of a CLSM allows for 3 dimensional reconstruction of dendritic spines (albeit this is also possible with serial EM sections, but using CLSM is significantly less labor intensive). Secondly, CLSM can be used to estimate the size of the dendritic spines in living cells (Hosokawa et al., 1995) which is particularly useful in demonstrating gradual morphological changes over time, whereas the use of EM requires fixation and processing of the cells.

1.5 Current methods of functional analysis

While the necessary tools for the structural examination of single CNS synapses have been available for decades (e.g. EM), the functional examination of single CNS synapses has become practical only in the past five years, due to the remarkable advances in recording and imaging technology.

1.5.1 Electrophysiology

Since, generation and propagation of action potentials are the defining characteristics of a neuron, our understanding of neuronal function is entirely indebted to the ability to measure electrical currents and potentials. This procedure was developed by Marmount (1949), Cole (1949), and Hodgkin et al. (1949). In principle, an electrolyte-filled glass electrode is used to measure the currents inside, on the membrane, or outside of a neuron. The most common variations of this approach are the gigaseal patch and the whole-cell recording (Hamill and Sakmann, 1981; Sakmann and Neher, 1983). In these techniques, the recording electrode forms a high resistance (gigaohms) seal with a patch of membrane of the cell body, and the patch is then excised from the cell (or ruptured so that the intracellular environment comes freely in contact with the solution in the electrode). Considering the large number of synaptic connections that a single CNS neuron makes, recording of the postsynaptic currents at the cell body does not allow for the resolution of electrical events to individual synapses. In essence, an electrical event can be attributed to a single synapse if either an identified synapse is activated while recording from the soma, or the recording electrode is placed directly on the postsynaptic membrane of a release site.

Liu and Tsien (1995) were the first group to study the properties of synaptic transmission at single synaptic boutons. In their experiments, they initially labeled synaptic terminals of hippocampal neurons grown in culture using the vital dye FM1-43. The styryl fluorescent dye FM1-43 stains the functional presynaptic release sites of a nerve terminal (for further information on FM1-43 see section 1.5.2). Once the release sites are identified, while recording the whole-cell currents at the cell body, the identified sites are locally perfused with a puffer pipette containing K^+ and Ca^{2+}. This results in depolarization of the labeled presynaptic terminal and the subsequent release of neurotransmitter from that terminal. Thus, the currents arriving at the soma immediately following the focal perfusion correspond to the response of a single synapse. Spontaneous events elsewhere are eliminated by superfusion of the neuron with a low Ca^{2+} containing solution (for synaptic transmission to occur Ca^{2+} must enter the presynaptic terminal). A particular drawback of this method is the use of cultures at very low density to ensure the activation of a single synapse by perfusion.

Another approach to selective activation of single synapses is to record from the soma of a postsynaptic neuron while simultaneously stimulating the presynaptic neuron (Miles et al., 1996). The postsynaptic currents that coincide with the stimulation of the presynaptic neuron are thus due to the single synapse activation, assuming that there is only one synaptic contact between the presynaptic and the postsynaptic neurons (the number of synaptic contacts can be determined by including fluorescent dyes in the patch solution). The requirement for a single synaptic connection makes this approach particularly difficult, since even in culture two neurons often form more than one synaptic contact with each other.

The most direct way of measuring the electrical activity of a single synapse is by recording from the postsynaptic membrane of a synapse prior to the conduction of the signal to the cell body (Forti et al., 1997). For this purpose, the presynaptic terminals are again prelabeled with FM1-43. While using the fluorescent signal to guide the electrode, the recording electrode forms a tight seal onto the postsynaptic dendrite. Thus, any currents detected by the recording electrode will represent the response of a single synapse.

As it is evident from the description of the above approaches, the electrophysiological analysis of a single synapse function is very difficult in practice. In the past decade, the advent of fluorescent indicators however, has opened a gateway to more direct techniques of functional analysis using imaging.

1.5.2 Imaging

Use of fluorescence in probing biological structures and activities is particularly rewarding since it often provides an excellent signal to noise ratio, and the signal can be measured continuously with high spatial and temporal resolution (Taylor et al., 1986). The earliest use of fluorescence was in immunocytochemistry in which the secondary antibodies were tagged with a fluorescent probe (Nairn, 1976). Presently, fluorescent probes can be used to assess morphology, measure diffusion properties, sense conformational changes, detect alterations of the membrane potential, and trace the dynamics of various intracellular ions (Tsien, 1989). For the purpose of this study, the review of imaging techniques will be limited to the dyes and the relevant fluorescent microscopic methods that are used in assessing synaptic function of a single synapse.

1.5.2.1 Fluorescent indicators

Measurement of the intracellular free Ca^{2+} concentration ($[Ca^{2+}]_i$) has by far provided the greatest insight into the understanding of synaptic transmission than any other ion. This importance stems from both the role of Ca^{2+} as a trigger of second messenger systems, as well as the fact that Ca^{2+} dynamics can indicate both synaptic and electrical transmission in a neuron (Denk et al., 1996). In principle, all Ca^{2+} indicators have an octacoordinate binding site for Ca^{2+}. Upon Ca^{2+} binding, the lone pair of electrons of nitrogen (part of the binding site) is diverted away from the aromatic system, resulting in a large shift in the emission spectra of the indicator (Tsien, 1980). Currently the most popular dyes for tracing $[Ca^{2+}]_i$ dynamics in neurons are fura-2, fluo-3, and calcium green-1. These dyes can be injected directly into a cell or used in a hydrolyzable acetoxymethyl (AM) ester form that is membrane permeable (Tsien, 1989). Measurement of the change in $[Ca^{2+}]_i$ in dendritic spines allows for the assessment of the activity of a single synapse.

While measuring the influx of Ca^{2+} into a spine is a reliable indicator of the postsynaptic membrane response of a single synapse (Murphy et al., 1994), this method does not provide any information regarding the presynaptic activity of the synapse. As previously mentioned, the significance of the presynaptic regulation of synaptic activity during plastic changes is still undetermined. In the past five years, the advent of FM1-43 has allowed for the investigation of the presynaptic plastic changes using imaging techniques. FM1-43 is a styrylpyridinium dye which can be used to map synaptosomal recycling in nerve terminals. The mechanism of action of FM1-43 is based on the high affinity of its molecules for lipid membranes (due to a hydrophobic tail) and the inability to completely penetrate the membranes because of the divalent cationic head (Betz et al., 1992). In order to examine synaptic function, the dye must be initially loaded into the presynaptic terminals. For this purpose, the dye is placed in the extracellular solution and the neurons are then stimulated. During stimulation the dye is trapped in recycling vesicles and is endocytosed into the nerve terminals. The free dye is then washed out of the extracellular solution by perfusion with a dye-free solution. The alignment of fluorescent patches with the postsynaptic densities proves the presence of the dye in recycled synaptic vesicles (Betz et al., 1992). Once the terminals are loaded, changes in fluorescence would represent synaptic release of vesicles, which in turn is indicative of presynaptic activity (Ryan et al., 1996; Murthy et al., 1997).

1.5.2.2 Imaging techniques

In order to detect a fluorescent dye, molecules of the dye must be initially excited by absorbing light of specific energy (or frequency). Following the excitation, the fluorophore molecules will return to their basal energy levels by emitting a light of specific frequency. Essentially, different imaging techniques use different ways of exciting and capturing the emitted light from the fluorophore (Pawley, 1995).

With the aid of intensified charge-coupled devices (CCDs), ordinary fluorescent microscopes can be used to spatially resolve synaptic spines emitting low levels of fluorescence (Murphy et al., 1994; 1995). CCDs are solid-state semiconducting devices that convert photons into electrical signals in response to illumination. The signals from an array of silicon photodiode sensors are intensified and displayed as an image (Inoué, 1986). In contrast, confocal microscopy (as described previously), with its ability to reject scattered (out of focus) light, allows imaging of dendritic spines within a brain slice (Alford et al., 1993; Jaffe et al., 1994); the resolution and contrast rapidly decrease with distance from the surface of the sample when using wide field imaging with a CCD camera. The property of a confocal microscope to reject scattered light results in the rejection of the light that originated from the sample but was scattered later along the path. Thus, when using a confocal microscope an increased number of excitations is required to provide an adequate number of detectable photons. This, in turn, results in greater photodynamic damage especially to a living specimen. Such a problem has been recently solved with the development of two-photon excitation laser scanning microscopy (Denk et al., 1996). In two photon laser scanning microscopy (TPLSM), a fluorophore is excited only when two infrared photons are absorbed almost simultaneously. The probability of simultaneous absorption of two photons by one molecule is quadratically dependent on the photon absorption cross section. Therefore, the excitation of a fluorophore is spatially restricted to a small volume. Photobleaching and phototoxicity occur only in the small excitation volume, while in single photon CLSM, they also occur in planes other than the focal plane (Svoboda, 1998).

1.6 Research Hypothesis

A single pyramidal neuron of the hippocampus or cortex can make up to 10,000 different synaptic connections (Amaral et al., 1990). Current hypotheses suggest that each of these connections is regulated independently (Frey and Morris, 1997) and most likely through alterations of synaptic structure (Stevens and Sullivan, 1998). Recent evidence suggests that families of proteins containing PDZ domains (protein binding sites involved in clustering of receptors at a synapse) such as PSD 95 and GRIP are involved in orchestrating the specific expression of glutamate receptors within a single synaptic contact (for a review see Sheng 1996). In addition, hypotheses involving the recruitment of new α-amino-3-hydroxy-5-methyl-4-isoxazole-propionic acid (AMPA; a subclass of ionotropic glutamate receptors) responsive synapses during LTP indicate that methods which can localize molecules to particular synapses are an essential complement to electrophysiology (Issac et al., 1995; Liao et al., 1995; Wang et al., 1996). For example, current studies suggest that a subset of apparently "silent" synapses lack AMPA glutamate-type receptors (ibid.). Although physiological studies were quite conclusive, they failed to determine whether AMPA receptors were expressed at the apparently silent synapses as it is possible that recruitment of new AMPA responsive synapses may involve the elaboration of new receptors or the modification of existing receptors. Ideally, to address these types of questions, it is necessary to assess the strength and the structure of the same synapse simultaneously. For this purpose, **we have developed two methods which enable the ultrastructural analysis and antibody staining of single electrophysiologically-characterized neurons. The first method (Chapter III)**

provides a three step approach to a) determining the activity of a single synapse using wide field Ca^{2+} imaging, b) measuring the spine size and distribution using CLSM (and possibly 3D reconstruction of the characterized synapse), and c) examining the ultrastructural properties, such as PSD size and the number of presynaptic vesicles, of the characterized synapse. In effect, we have been able to take advantage of both confocal and electron microscopy to describe the structure of a single synapse. **The second method (Chapter IV) allows for the examination of receptor composition of a functionally characterized synapse.** The reason for using this technique is that when using anything but an extremely low density culture of neurons (Craig et al., 1993), it is virtually impossible to make a cross correlation between antibody staining and activity observed on a fine dendrite or axonal process measured using optical techniques such as Ca^{2+} imaging (because many processes are stained). Calcium imaging techniques enable single synapses to be studied since they allow an investigator to fill a single neuron (using intracellular or patch electrodes) with a calcium-sensitive probe thus reducing background fluorescence signals from other neurons (Malinow et al., 1994; Murphy et al., 1994; Yuste and Denk, 1995). We have used the advantage of single cell filling in immunostaining studies. Our method involves local production of H_2O_2, which acts as a substrate for a peroxidase-mediated antibody staining reaction. This reaction can occur within a single neuron that has had synaptic responses mapped along its dendrites using Ca^{2+} imaging.

Chapter II

Materials and Methods

2.1 Cell Culture

Cortical or hippocampal neurons and glia were dissociated from 17-18 day gestation rat fetuses, placed in culture, and allowed to mature for 17-26 days in vitro as described by Murphy and Baraban (1990). The dissociated cells were resuspended at a density of 1.2×10^6 cells/ml in minimal essential medium (MEM) supplemented with 5.5 gm/L glucose, 2 mM glutamine, 10% fetal calf serum, 5% heat-inactivated horse serum, 50 U/ml penicillin, 300 μM L-cystine, and 0.05 mg/ml streptomycin; plated onto polylysine-coated (10 μg/ml) 35 mm culture dishes in 1.5-2 ml of medium, and placed in a 37°C CO_2-buffered incubator. For imaging purposes, the plastic bottom of culture dishes was replaced by polylysine-coated Aclar fluoropolymer film (Alliedsignal Inc., Pottsville, PA). The cultures were fed by addition of MEM with 5.5 gm/L glucose, 5% heat-inactivated horse serum, and 2 mM glutamine, after about 4-6, 12-14, 16-17, and 19-21 days in culture, by removal and replacement of approximately 60% of the medium.

2.2 Intracellular calcium imaging and analysis

In experiments in which synaptic function was assessed, neurons were filled with fluo-3/mag-fura-2 and biocytin under whole-cell recording mode using patch-clamp pipettes (~ 7-10 MΩ). The patch pipette solution contained 1.6% biocytin, 0.3 mM fluo-3 (K^+ salt) in combination with 1.0 mM mag-fura-2 (used to view basal fluorescence), 61 mM K^+ $MeSO_4$, 5 mM Mg-ATP, 0.3 mM GTP, 20 mM NaCl, and 10 mM HEPES (pH

7.2). The following magnesium-free extracellular solution was then used to isolate and view local Ca^{2+} transients miniature synaptic activity: 137 mM NaCl, 5.0 mM KCl, 5.0 mM $CaCl_2$, 0.34 mM $Na_2HPO_4(H_2O)_7$, 10 mM Na^+-HEPES, 1mM $NaHCO_3$, 20 μM picrotoxin, 0.3 μM TTX, 22 mM glucose (pH 7.4; 310 mOsm). Using video imaging of $[Ca^{2+}]_i$ with 33 ms temporal resolution, as previously described by Murphy et al. (1994, 1995), miniature synaptic calcium transients were detected in a subset of the dendritic arbor. A fiber optically coupled intensified CCD camera with a Gen III intensifier tube was used for all experiments (Stanford Photonics, Palo Alto, CA) in combination with an Epix 4M12-64 MB frame grabber board. Images were analyzed on a Pentium microcomputer using custom routines written in the program IDL (Research Systems Inc., Boulder, CO).

2.3 Confocal Microscopy and Analysis

Cells were fixed with 4% paraformaldehyde and 0.2% glutaraldehyde in 0.1 M Sörensen's Na^+ phosphate buffer (pH 7.2-7.4, 1 hr at room temperature). After several rinses with PBS cells were treated with 0.2% Triton X-100 for 4 min, washed with PBS (3-5 vol. over 5 min) and blocked with 3% normal goat serum overnight at 4°C. During rinses and the incubations cells were continuously agitated. Subsequently, cells were washed with PBS (3-5 vol. over 5 min), incubated with avidin-fluorescein (5 μg/ml; Molecular Probes) in the presence of 1% BSA (1 hr, at room temperature). After rinsing with PBS, cells were mounted on a glass slide with Slow Fade™ anti-fade reagent in PBS (Molecular Probes). Fluorescein-labeled neurons (or fluorescein beads from Molecular

Probes) were examined using a Bio Rad MRC-600 CLSM, attached to a Zeiss Axioskop. Argon laser was used with 488 nm excitation filter and <514 emission filter (BHS block). Optical sections of the area of interest were scanned using 100X objective at a regular increments of 0.54 µm. Frames collected in z-series were saved in the Bio Rad file format on a 486 IBM microcomputer. A 2-D reconstruction of the area of interest was made by summation of the maximal z-projection stacks. From the projected image, the number of spines and the size of the spine heads (number of pixels spanning the spine head) within the area of interest were determined using the Adobe Photoshop Graphics software (Adobe Systems Incorporated).

2.4 Electron microscopy

Following CLSM cells were rinsed with PBS, pre-incubated with 3% normal goat serum (1 hr at room temperature) and incubated with biotinylated anti-Avidin (1:5000; Pierce) over night at 4°C. Avidin-immunoreactivity was visualized using the ABC technique and DAB/Ni/H_2O_2 (see the section on single cell staining for the protocol). EM was also used to examine cells stained using the single-cell staining procedure. Subsequent to DAB staining, cultures were extensively washed with PBS (5 x ~3 mls over 30 min, at room temperature), followed by further fixation in 2.5% glutaraldehyde in 0.1 M Sörensen's Na^+ phosphate buffer (pH 7.2-7.4, 1 hr on ice), washing in the same buffer (3 vol. over 30 min, on ice), overnight incubation in fresh buffer (4°C), and then postfixation in 1% OsO_4 in the same buffer (1 hr, on ice). Following a final buffer wash (3 vol. over 30 min, on ice), cultures were dehydrated in a graded ethanol series (50%, 70%, 85%, 95%, 100%) and flat embedded in Spurr resin on Aclar plastic. Subsequently, areas containing DAB/Ni stained neurons were excised, separated from Aclar, and mounted on blank blocks. Serial sections of approximately 70 nm thickness were collected on Formvar-coated single slot grids, stained with 2%-3% aqueous uranyl acetate followed by Reynold's lead citrate (Reynolds, 1963), and then examined at 80 kV in a Zeiss EM 10C STEM.

2.5 Assay of glucose oxidase distribution

The underlying basis for the proposed single cell staining technique is local generation of H_2O_2 within the entire cell of interest. Hence it is imperative that GO is distributed uniformly in the cell of interest. The distribution of GO was assessed by avidin-peroxidase staining of biocytin-filled cells. Neurons were injected with biocytin, incubated with avidin conjugated GO (90 μg/ml; Vector Laboratories) followed by biotinyated peroxidase (1:65 dilution of solution B from the Vector ABC kit), and stained with glucose-containing, H_2O_2-free diaminobenzidine (DAB) solution (for protocol see section on Single Cell Staining). Staining pattern of avidin in the cells represents the distribution of GO (avidin is conjugated to GO; the source of H_2O_2 for the reaction). This assay was used to determine the effects of various fixation protocols (1 hour fixation with 4% formaldehyde, or 4% formalin, or 4% formaldehyde with 0.2% glutaraldehyde all in 0.1 M Sörensen's Na^+ phosphate buffer) as well as the duration of incubation periods on the GO distribution within a single cell.

2.6 Immunofluorescent staining of neuron-specific enolase

Cells were fixed with 4% paraformaldehyde in 0.1 M Sörensen's Na^+ phosphate buffer (pH 7.2-7.4, 1 hr at room temperature). After several rinses with PBS cells were treated with 0.2% Triton X-100 for 5 min, washed with PBS (3-5 vol. over 5 min), pre-incubated with 3% bovine serum albumin (1 hr at room temperature) and incubated with 1:4000 rabbit anti-neuron specific enolase (Polysciences Inc., Warrington, PA), and 2% bovine serum albumin over night at 4°C. Cells were then rinsed in PBS (30 min, 3 changes) and incubated for 1 hr at room temperature with fluorescein conjugated goat anti-rabbit IgG (1:100; Vector Laboratories) and 10 μg/ml Texas Red conjugated avidin (Vector Laboratories). Finally cells were washed with PBS (30 min, 3 changes), and mounted on a microscope slide with anti-fade mounting reagent (Molecular Probes). The cultures labeled with the two fluorophores were examined with a Bio Rad MRC-600 confocal laser scanning microscope. The A1 and A2 filter blocks, supplied with the microscope, were used to specifically examine fluorescein and Texas Red fluorescence. At gain settings and the filter block used to detect Texas Red fluorescence, no fluorescein signal was detected, and vice versa.

2.7 Single cell staining

Based on the results of GO distribution (Figure-2), the following protocol was devised for visualization of antibody reactivity in single neurons. Neurons were filled with fura-2 and biocytin for ~2 min using patch-clamp pipettes (~ 10-12 MΩ). The patch pipette solution contained 1.6% biocytin, 1 mM fura-2 (used to view live cell morphology under fluorescence), 61 mM K^+ $MeSO_4$, 5 mM Mg-ATP, 0.3 mM GTP, 20 mM NaCl, and 10 mM HEPES (pH 7.2). After the injection cells were fixed with 4% paraformaldehyde in 0.1 M Sörensen's Na^+ phosphate buffer (pH 7.2-7.4, 1 hr at room temperature). After several rinses with PBS cells were treated with 0.2% Triton X-100 for 5 min, washed with PBS (3-5 vol. over 5 min), pre-incubated with 3% bovine serum albumin (1 hr at room temperature) and incubated with avidin conjugated GO (90 μg/ml; Vector Laboratories), desired primary antibody, and 2% bovine serum albumin over night at 4°C. The primary antibodies used include rabbit anti-neuron specific enolase (1:4000; Upstate Biotechnologies Inc., Lake Placid, NY), and rabbit anti-GluR 2/3 (1:100; Upstate Biotechnology Inc., Lake Placid, NY). Cells were then rinsed in PBS (30 min, 3 changes) and incubated for 5 hr at room temperature with peroxidase conjugated goat anti-rabbit IgG (1:100; Vector Laboratories). After further PBS rinsing (30 min, 3 changes) cells were incubated in 5 mls of staining solution containing 0.1 mg/ml diaminobenzidine (DAB), 1.7 mg/ml D-glucose (diluted from 10 mg/ml stock made at least 24 hrs earlier in 50 mM tris buffer to allow for mutarotation to β-D-glucose), 50 mM imidazole and 10 mg/ml nickel ammonium sulphate in tris buffer (50 mM tris, pH 7.6). The staining reaction was regularly monitored over the course of 1-3 hours to prevent overstaining.

2.8 Conjugation of catalase beads

Catalase (Sigma Chemical Company, St. Louis, MO) was conjugated to agarose beads (100 μg of catalase per 100 μl of beads) using the SulfoLink® Coupling Gel

(Pierce, Rockford, IL). The peroxide clearance activity of the beads were assayed using the o-dinisidine method of Maehly and Chance (1954): substrate solution consisted of one volume of 240 U/ml horseradish peroxidase (HRP) in sodium citrate buffer and one volume of 2 mM o-dianisidine. The quenching solution contained 10 μl of beads or 10 μg of catalase added to 1 ml of 100 μM peroxide. The reaction was started by adding beads or catalase to the peroxide. At various time intervals, 100 μl of the quenching solution was added to 400 μl of the substrate solution, and the absorbance of the resultant solution was measured at 450 nm.

CHAPTER III

A 3 step approach to correlative functional and structural analysis of single CNS synapses

3.1 Resolution of wide-field microscopy versus confocal microscopy

The principle of confocal microscopy is based on elimination of out of focus light from the image. Inherent in this filtering process is the reduction of noise and the apparent increase in resolution especially in thick specimens. In order to determine whether or not when imaging primary cultures of 2-3 cells in thickness a confocal microscope will still provide better images of fine structures than a CCD camera, we measured the lateral resolution of our CCD camera and our confocal microscope. A simple way of estimating the lateral resolution is to determine the half-maximal intensity distance. This is the distance away from a fluorescent point source at which the intensity of the emitted light is half of the maximal intensity. For this purpose, fluorescein-labeled microspheres of 200 nm diameter were imaged using both systems and the averaged (or confocal summation of maximal z-projections) images were analyzed using the IDL analysis software. From each averaged image, a single bead of submaximal (<250) pixel intensity was chosen, and a plot of distance (across the image) against pixel intensity across the bead was obtained (Figure-1A and 1B). Using this plot, it is evident that the half-maximal intensity band width (i.e. the number of pixels with an intensity greater than the half-maximal intensity) is slightly greater for a CCD camera (Figure-1B) than for a confocal microscope (Figure-1A). This difference is better illustrated when the distance (from the point of 100% intensity) is plotted against the normalized intensity (Figure-1C). The thick trace is the normalized intensity curve for the CCD camera, and the thin trace is

Figure-1. Measurement of the lateral resolution of the wide-field and confocal microscopy.

(A) Plot of pixel value (intensity) of a 200 nm diameter fluorescein microsphere against the distance across the image. A single bead was imaged using a CLSM. A straight line is drawn to indicate the half-maximal intensity. The number of pixels with values greater than the half-maximal intensity represents the half-maximal band width for this confocal microscope.

(B) Plot of pixel value (intensity) of a 200 nm diameter fluorescein microsphere against the distance across the image. A CCD camera was used to image a single bead under a wide-field microscope. A straight line is drawn to indicate the half-maximal intensity.

(C) Pixel values for each pixel were normalized for the two beads imaged in (A) and (B), and were plotted against the distance away from the point of maximal intensity. This distance is calculated based on a calibration of 0.2 μm in length/pixel in our system. The thick trace is the normalized intensity curve for the CCD camera, and the thin trace is the normalized intensity curve for the confocal microscope.

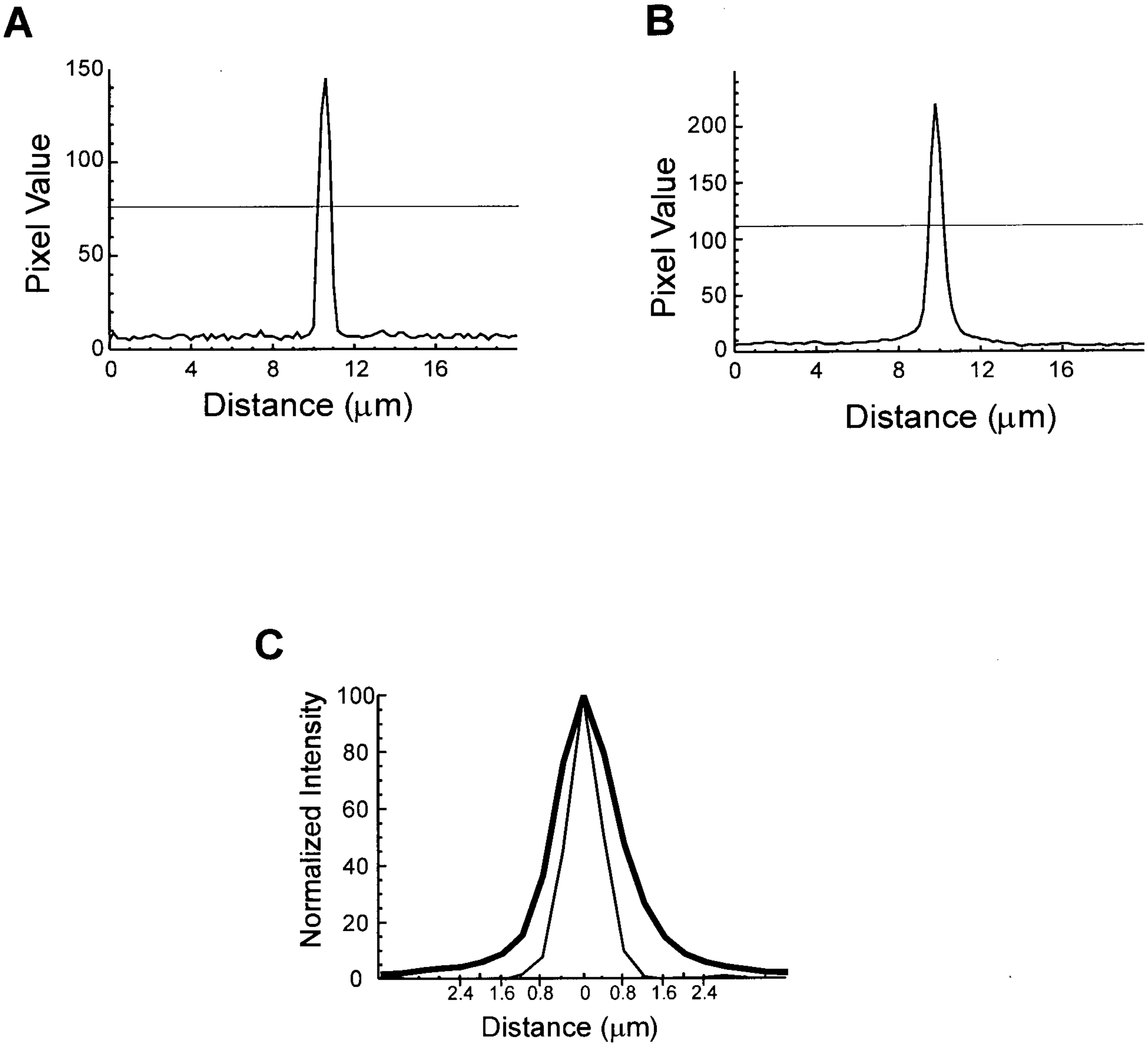
A
Pixel Value
150
100
50
0
0
4
8
12
16
Distance (μm)
B
Pixel Value
200
150
100
50
0
0
4
8
12
16
Distance (μm)
C
Normalized Intensity
100
80
60
40
20
0
2.4
1.6
0.8
0
0.8
1.6
2.4
Distance (μm)

the normalized intensity curve for the confocal microscope. Considering that each pixel is approximately 0.2 μm in length (based on the specifications of our systems), the half-maximal intensity width of our confocal microscope was determined to be 0.8 μm (4 pixels), in contrast to 1.2 μm (6 pixels) for our CCD camera. Measurement of the axial (z-axis) resolution is considerably more complex than the lateral resolution, and it is beyond the scope of this study.

3.2 Correlative functional and structural analysis

Our 3-step method of analysis allows for the measurement of miniature Ca^{2+} transients in dendritic spines as an index of synaptic function using wide-field microscopy, followed by the measurement of the size of identified spines (and if desired reconstruction of the spines in 3D) using CLSM, and finally ultrastructural examination of the same spines with an EM. An example of the application of this novel approach is shown in Figure-2. A single rat cortical neuron in culture was injected with biocytin, mag-fura-2 and fluo-3. Mag-fura-2 which is a Ca^{2+} indicator of low affinity was used to provide a fluorescent image of the cell at resting Ca^{2+} level (Figure-2Aa and 2Ab). Fluo-3 was used to detect miniature synaptic calcium transients (MSCTs) since it has a high affinity for Ca^{2+} and thus it reliably detects small changes in $[Ca^{2+}]_i$ levels. Ca^{2+} transients were considered to be MSCTs if at least four consecutive measurements from 33 msec video frames were more than 1 SD above the baseline noise. Using the CCD camera, 11 trials of 10 seconds duration were recorded from a small area of interest (Figure-2Ab). Upon analysis of the data, four individual synaptic sites were identified to be active during the 110 seconds of

Figure-2. Correlative functional and structural examination of single CNS synapses.

(Aa) Composite fluorscence image of a live cultured cortical neuron filled with mag-fura-2, fluo-3, and biocytin. Boxed area indicates the region imaged during the experiment. Scale bar 15 μm.

(Ab)(top) Averaged mag-fura-2 fluorescence image of area of interest captured by a CCD camera. Imaging for miniature synaptic Ca^{2+} transients revealed four distinct active synapses (as indicated by the arrows) during 11 trials of 10 second duration. Scale bar 5 μm. (middle) Confocal maximal intensity projection image of the area of interest. Subsequent to $[Ca^{2+}]_i$ imaging, the biocytin injected cell was fixed, incubated with avidin fluorescein, and examined with confocal laser scanning microscopy. Scale bar 5 μm. (bottom) Photograph of the area of interest DAB stained for avidin immunoreactivity. The cell was then processed for EM analysis. Scale bar 5 μm.

(B) Plots of $[Ca^{2+}]_i$ versus time, made from four different dendritic regions indicated by arrows, are shown during eleven overplotted 10 sec sampling epochs. The thick traces represent the trials during which a miniature synaptic calcium transient was detected. Other changes in the $[Ca^{2+}]_i$ are not considered to be miniature synaptic calcium transients as they are less than 1 SD above the baseline noise in magnitude.

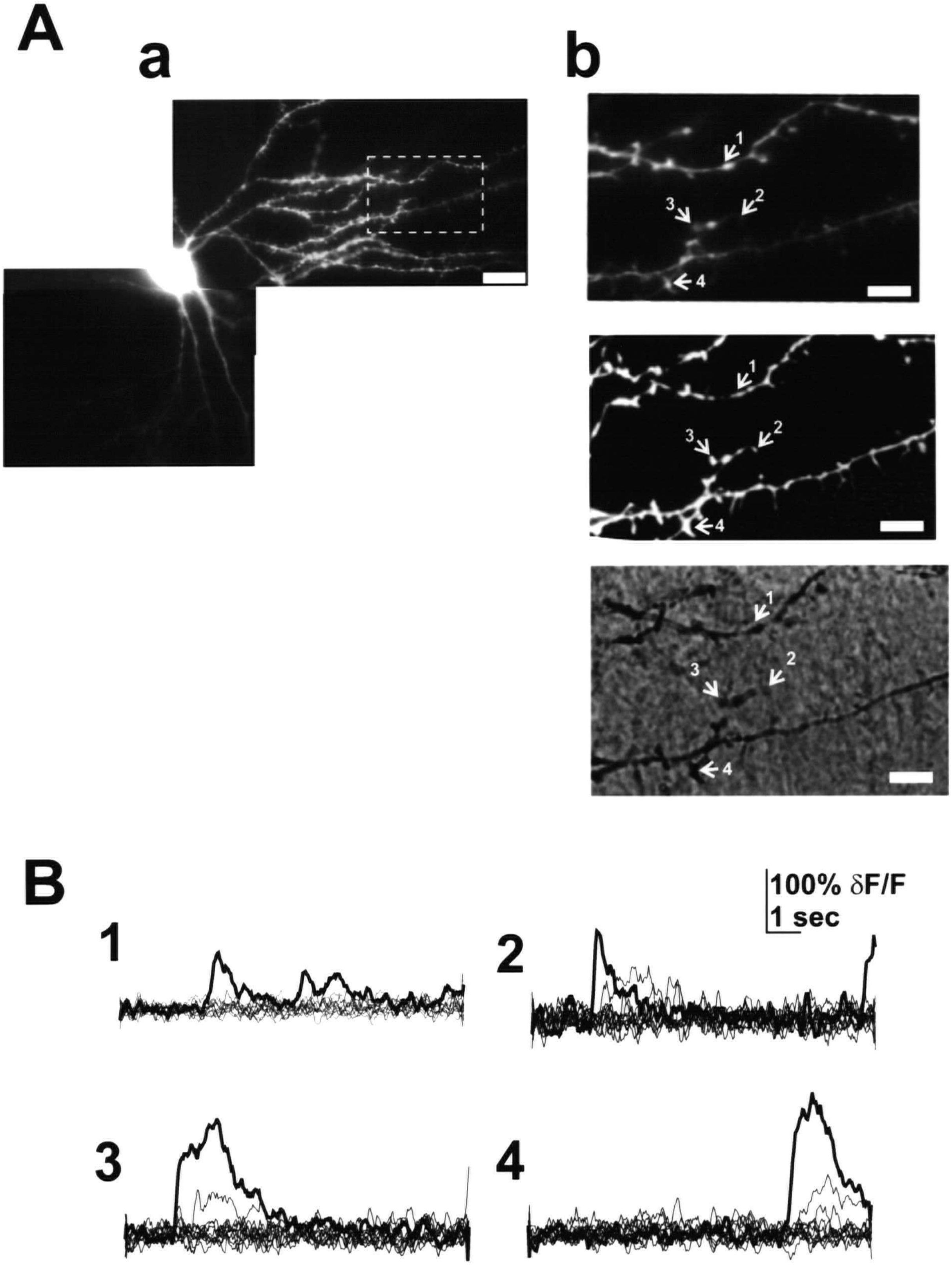
A
a
b
1
2
3
4
B
100% δF/F
1 sec
1
2
3
4

imaging (Figure-2B). Following the functional study, the cell was labeled with fluorescein and examined using a confocal microscope (Figure-2Ab). Analysis of the confocal images revealed that the dendritic spines of active synapses varied in size (Table-1). In this analysis, the cross sectional area of sites 2 and 3 were calculated by counting the number of pixels covering the head of the spines in the projection image. As previously mentioned, based on the specifications of our confocal microscope each pixel is 0.2 μm in length, and thus, the area of a single pixel is 0.04 μm^2. No attempt was made to calculate the cross sectional areas of spines 1 and 4, since their boundaries could not be defined as the heads of these spines lie directly above a dendrite. It must be emphasized that estimation of the spine size was conducted in order to illustrate the compatibility of our method with the use of confocal microscopy in structural analysis. Hence, any inferences with regards to correlation between spine size and synaptic activity must be made based on further investigation. A comparison between the confocal image and the wide-field image obtained using the CCD reveals that many of the spines imaged with the CCD camera lie on focal planes other than that of the main dendrites. Hence, these spines appear out of focus in wide-field images. In contrast, all the spines are in focus in the confocal image since the presented image is a stacked projection of several images taken at sequential focal planes. Finally, the cell of interest was subjected to DAB/peroxidase staining (Figure-1Ab), and was successfully processed for EM examination (electron micrographs not shown). Electron microscopy is essential in revealing the size of the presynaptic vesicle pool of the identified synapses.

Table 1.
Measurement of spine sizes of functionally characterized synapses.

Site Number[a]	Number of pixels[b]	Cross sectional area (μm^2)[c]	Volume (μm^3)
2	33	1.32	1.14
3	60	2.40	2.80

[a] Imaging for miniature synaptic Ca^{2+} transients revealed four distinct active synapses. Synapses numbered 2 and 3 were selected for structural examination.

[b] The number of pixels covering the head of the two spines in the confocal projection image was counted.

[c] Based on the specifications of our confocal microscope each pixel is 0.2 μm in length, and thus, the area of a single pixel is 0.04 μm^2.

CHAPTER IV

Restriction of peroxidase-mediated antibody reactivity to single neurons by local H_2O_2 production

4.1 Local generation of H_2O_2 by glucose oxidase

Peroxidase-linked antibody staining techniques permit a signal derived from antibody binding to be amplified through enzymatic reduction of DAB. This method has many advantages over fluorescence detection of antigens such as high sensitivity, excellent spatial resolution and the ability of signals to be further investigated at the EM level (Fonseca and Brown, 1997). Therefore, we have chosen to modify this procedure to permit better resolution of neuronal processes by restricting antibody mediated staining to a single neuron. The principle of our method is to generate H_2O_2, which is essential for the DAB mediated staining reaction in only a neuron of interest. As depicted in Figure-3, this is accomplished by first loading a neuron of interest with biocytin, and then exposing the permeabilized cell to avidin linked glucose oxidase (GO). In the presence of glucose in the medium, H_2O_2 generation and peroxidase mediated staining is restricted to a single cell.

4.2 Optimal duration of GO incubation

As the underlying basis of our single cell antibody staining technique is local generation of H_2O_2 by biocytin coupled GO (within the cell of interest), it is imperative to ensure that GO is distributed uniformly within the cell. One important factor in determining the distribution of GO is the rate of diffusion of avidin conjugated glucose oxidase (Av-GO) into permeabilized cells, which in turn governs the necessary

Figure-3. Schematic representation of single cell staining.

Injection of biocytin into the cell of interest allows for selective binding of avidin conjugated glucose oxidase (Av-GO; see injected cell). In the presence of glucose, Av-GO produces H_2O_2, which is a substrate for diaminobenzidine (DAB) staining reaction,. The binding of primary (1° Ab) and peroxidase conjugated secondary (perox-2° Ab) antibodies to non-injected cells, does not result in staining since there is no source of H_2O_2.

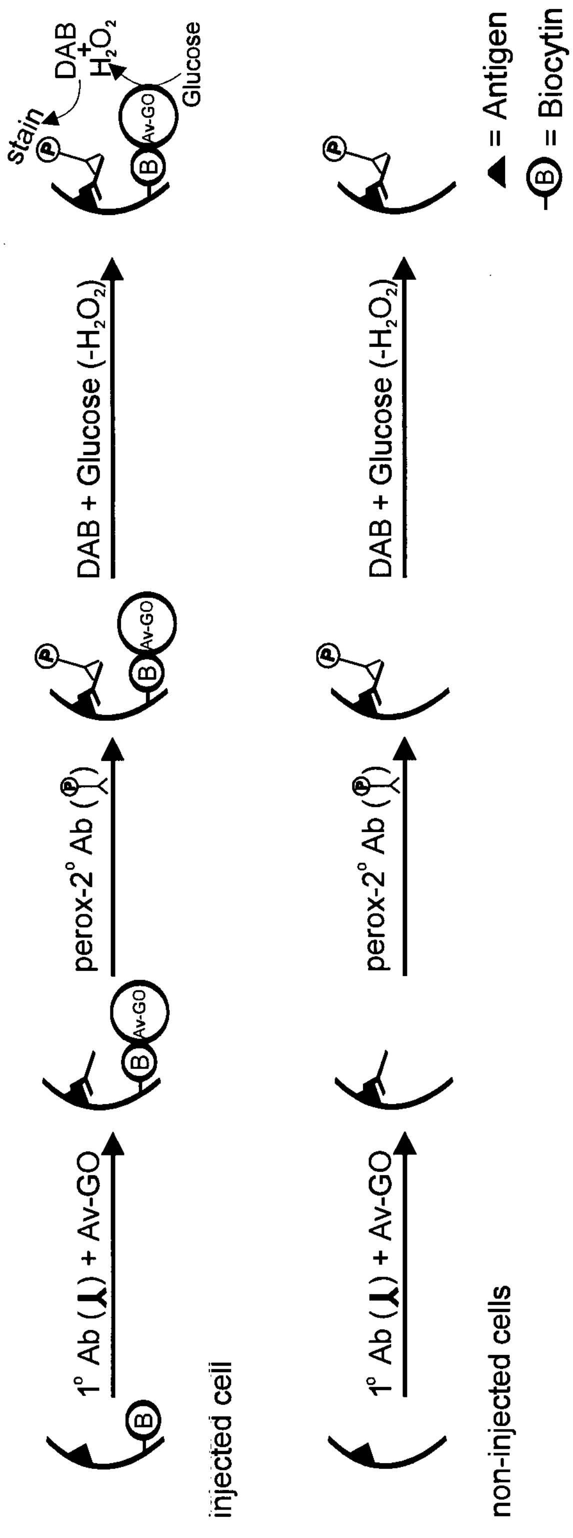
1° Ab ( ) + Av-GO
B
Av-GO
perox-2° Ab ( )
P
DAB + Glucose (-H2O2)
stain
DAB
+
H2O2
Glucose
injected cell
non-injected cells
= Antigen
B = Biocytin

incubation period for Av-GO. Using an assay of GO distribution (see Materials and Methods) a time course for the penetration of Av-GO into the cell of interest was determined (over a period of 1-12 hrs; data not shown). In this assay, which is dependent on biotinylated peroxidase, the resulting staining represents the distribution of avidin within the injected cell. Since cells were only incubated with Av-GO, the staining must also be indicative of the GO distribution. Furthermore, using a glucose containing DAB solution without H_2O_2, we also verified that the localized GO was also functional. Based on our experiments, we conclude that GO must be incubated overnight (~12 hrs) along with primary antibody in order to obtain uniform penetration throughout the entire cell, including the distal/fine processes and spines.

4.3 Effect of fixative on GO distribution

Using cells injected with fura-2 and biocytin, we examined the effects of various fixation protocols on the distribution of GO. After obtaining fluorescent images of the soma and dendrites, neurons were fixed and assayed for the distribution of GO (Figure-4). GO was found to be distributed uniformly throughout the cell following formalin or paraformaldehyde fixation (Figure- 4A & 4B). In glutaraldehyde fixed cells, however, the distribution of GO was non-uniform (Figure-4C). Based on this result, all subsequent staining experiments were performed on paraformaldehyde fixed cells.

Figure-4. The distribution of glucose oxidase-dependent staining within a cell is dependent on the fixation method.

(A) (left) Composite fluorescence image of a live cultured cortical neuron filled with fura-2 (fluorescent) and biocytin. (right) DAB mediated staining of the fixed cell. Following imaging, the cell was fixed with paraformaldehyde, permeabilized, and incubated with avidin conjugated to glucose oxidase (Av-GO) for ~15 hrs. After extensive washing biotinylated peroxidase was added followed by addition of glucose containing DAB (as described in the Methods).
(B) (left) Fura-2 image of live neuron. (right) DAB stained photograph of the fixed biocytin-filled cell. Following imaging, the cell was fixed with glutaraldehyde, permeabilized, and incubated as described in (A) and in the Methods.
(C) (left) Fura-2 live image of neuron. (right) DAB stain of the fixed cell. Following imaging, the cell was fixed with formalin, permeabilized, and incubated as described above. Scale bars 20 μm in all images.

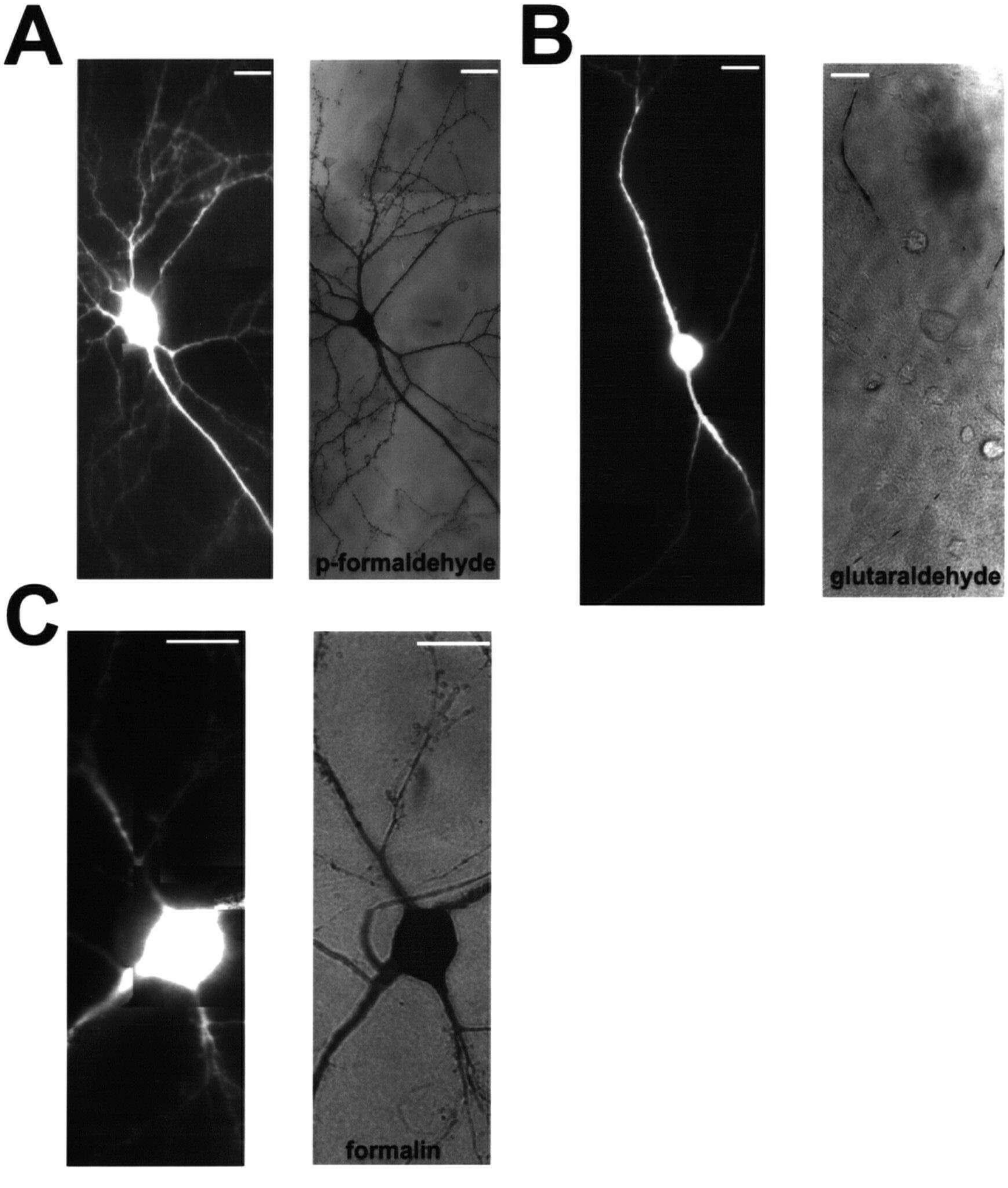
A
p-formaldehyde
B
glutaraldehyde
C
formalin

4.4 Fluorescence double labeling lacks resolution of DAB mediated single staining

Neuron-specific enolase (NSE) is a cytoplasmic enzyme which is highly expressed in neurons and some glia (Trapp et al., 1981; Vinores et al., 1984). Since NSE is present abundantly in neurons and their processes, it was considered to be the antigen of choice for examining the specificity and reliability of the method. In order to illustrate the advantage of our novel single cell staining method we initially attempted to localize NSE within a single neuron using conventional methods of fluorescence double-labeling. In these experiments a neuron of interest was initially injected with biocytin. Texas Red conjugated avidin was then applied to the fixed specimen in order to fluorescently-label the cell of interest (Figure-5A). Subsequently, cells were stained for NSE using a fluorescein-labeled secondary antibody (Figure-5B). The localization of NSE within the cell of interest can be defined by superimposition of images from the Texas Red-selective filter set and the fluorescein-selective filter set. Although staining of the soma was readily apparent, it was practically impossible to resolve dendritic NSE-immunoreactivity in the cell of interest from that of its neighbors. Our results indicate that despite the use of confocal microscopy, it is not possible to resolve antibody staining in fine cellular structures such as dendritic spines and small processes within a cell of interest using double-labeling methods.

4.5 Staining of single neurons for antibody reactivity

To better resolve fine subcellular details of antibody-mediated staining, we have used our method to locally generate H_2O_2, and restrict peroxidase-mediated staining to a cell of interest. For this purpose single neurons were coinjected with 1.5% biocytin and 1

Figure-5. Localization of neuron-specific enolase using immunofluorescence double labeling.

(A) Image of a fixed neuron filled with biocytin and incubated with avidin conjugated to Texas Red for 1 hour and imaged using confocal microscopy. Scale bar 20 μm.
(B) Averaged fluorescence image of the same cell and surrounding region (shown in A) stained for neuron-specific enolase. The fixed neuronal culture (from (A)) was incubated with anti-neuron-specific enolase overnight and visualized using a fluorescein conjugated secondary antibody with confocal microscopy. Scale bar 20 μm.

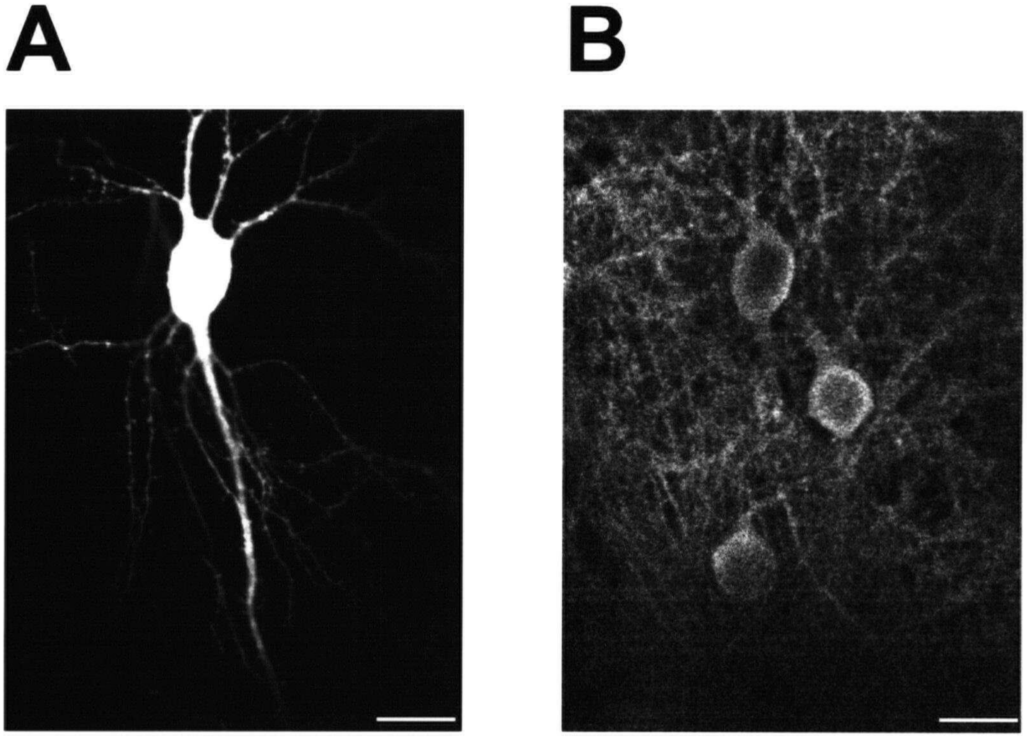
A
B

mM fura-2. Biocytin provides the means for binding Av-GO and fura-2 allows dendritic structures and potentially synaptic events to be evaluated in live cells using fluorescent microscopy (Figure-6A). Following the collection of fluorescent images, cells were fixed and stained for NSE using our single cell antibody staining method (Figure-6B). As illustrated in Figure-6 both main and fine processes were intensely stained for NSE. Examination of the staining at high magnification indicates that non-specific staining of processes of the neighboring cells does not occur. Staining of processes belonging to neighboring cells could occur if diffusion of H_2O_2 from the injected cell was extensive. In order to prove that despite the staining of a single cell, other NSE-immunoreactive processes were also present in close contact with the cell of interest, conventional H_2O_2 containing DAB/Ni staining was used after single-cell staining (Figure-6C). This method is applicable since all NSE-immunoreactive neurons have bound peroxidase but do not necessarily have a source of H_2O_2 generation (restricted to biocytin injected cells). As shown in Figure-6C, the cell of interest is surrounded by NSE-containing cells whose processes entangle the cell of interest. It is evident that the localization of NSE within a single neuron in high density cultures is not feasible using conventional peroxidase (Figure-6C) or fluorescence (Figure-5B) immunocytochemistry. Other preparations such as brain slices or slice cultures in which an even thicker neuropil is present would certainly benefit from our method.

4.6 Specificity of single cell method at the ultrastructural level

Localization of NSE within a neuron using our single cell method demonstrated that staining at light microscopic level is restricted to the cell of interest. It is however

Figure-6. Localization of neuron-specific enolase using single cell staining.

(A) (top) Composite fluorescence image of live neuron filled with fura-2 and biocytin. Scale bar 20 µm. (middle) Enlarged image of box 1 from (A) showing finer dendritic processes and spines. Scale bar 10 µm. (bottom) Enlarged image of box 2 from (A). Scale bar 5 µm.

(B) (top) Composite photograph of the same neuron DAB-stained for neuron-specific enolase (NSE) using single-cell staining. Scale bar 20 µm. (middle) Enlarged image of box 1 from (A). Scale bar 10 µm. (bottom) Enlarged image of box 2 from (A). Scale bar 5 µm.

(C) (top) Composite photograph of the same neuron DAB-stained for neuron-specific enolase (NSE) using conventional staining procedures performed after the single-cell staining of the injected neuron (H_2O_2 was added to DAB containing buffer). Conventional DAB mediated immunostaining indicates the presence of NSE in neighboring cells. Scale bar 20 µm. (middle) Enlarged image of box 1 from (A). Scale bar 10 µm. (bottom) Enlarged image of box 2 from (A). Scale bar 5 µm.

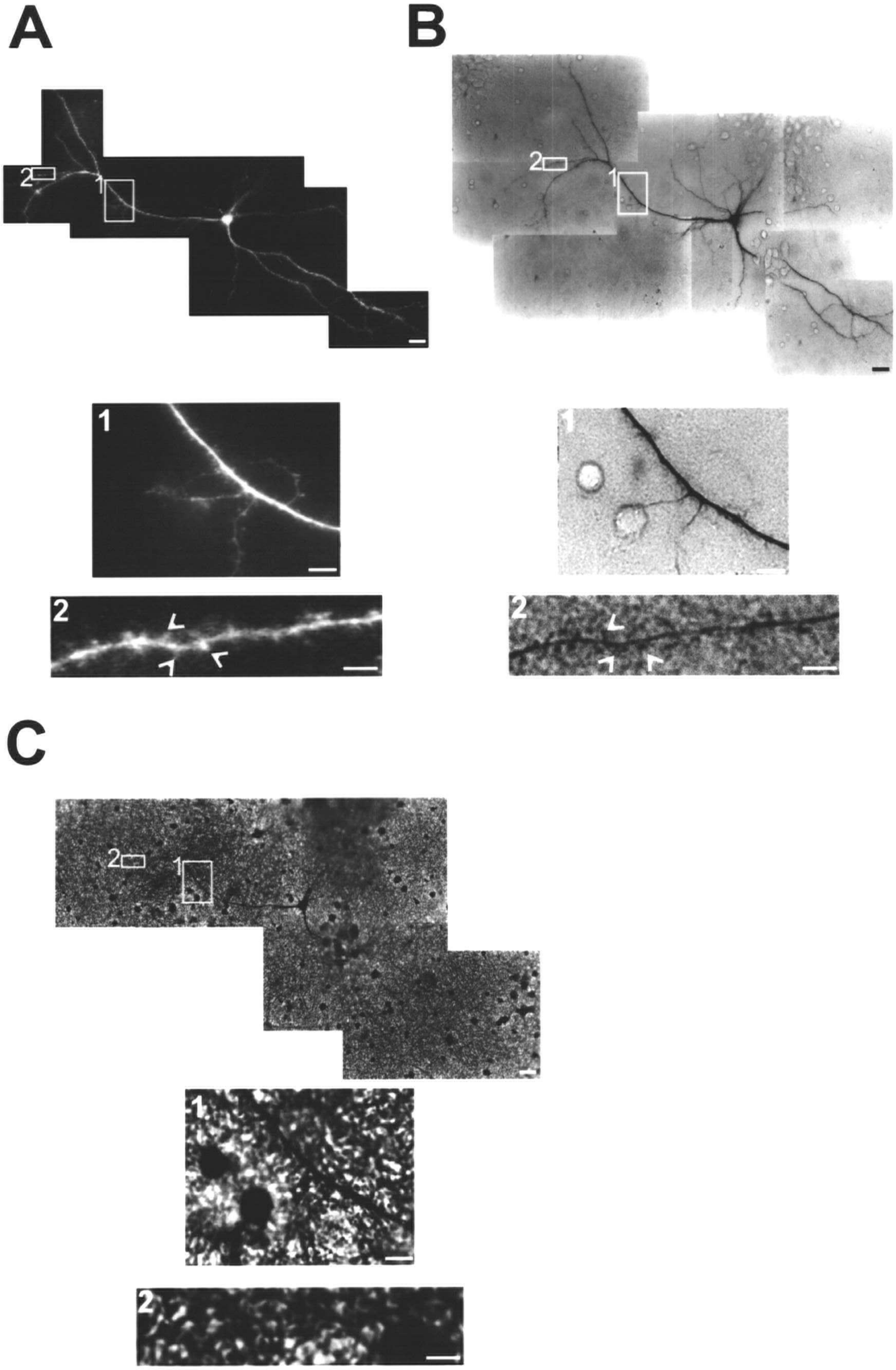
A
2
1
1
2
B
2
1
1
2
C
2
1
1
2

conceivable that some non-specific staining (of other cells) may have occurred but the signal was not detectable at the light microscopy level. For this reason, as well as the notion that single cell staining may be used to localize receptors to individual synapses, we examined our novel method using electron microscopy. In Figure-7 a cell was coinjected with fura-2 and biocytin. After capturing fluorescent images, the hippocampal neuron was fixed and immunostained for GluR 2/3 subunits. GluR 2/3 subunits are found in AMPA type glutamate receptors (Hollmann and Heinemann, 1994). As shown in Figure-7B, the GluR 2/3 staining was restricted to the cell of interest at the light microscopic level. Further examination of the stained dendrites using electron microscopy revealed no evidence of non-specific staining (of neighboring cells) in close proximity to the stained cell of interest (Figure-7C & 7D).

4.7 Detection of single quantal synaptic responses and AMPA-type glutamate receptor subunits at single synapses

By imaging $[Ca^{2+}]_i$ under conditions that both isolate miniature excitatory activity and promote Ca^{2+} entry through NMDA receptors (solution with TTX and no added Mg^{2+}), we have previously observed $[Ca^{2+}]_i$ transients that were attributed to miniature synaptic activity (Murphy et al., 1994). Miniature synaptic activity results from the spontaneous release of putative single quanta of transmitter. Evidence linking the local $[Ca^{2+}]_i$ transients to miniature synaptic activity was the sensitivity of the transients to NMDA receptor antagonists, and the observation that the transients were correlated temporally with spontaneous inward currents with characteristics similar to miniature activity (Murphy et al., 1994; Murphy et al., 1995).

Figure-7. Specificity of single cell staining demonstrated using electron microscopy.

(A) Composite image of live hippocampal neuron filled with fura-2 and biocytin. Scale bar 10 μm.
(B) Composite photograph of a cultured hippocampal neuron DAB stained for GluR 2/3 subunits using single-cell staining. Boxed area indicates area was examined at EM level. Scale bar 10 μm.
(C) Low magnification electron micrograph of the area in box 1 from (B) showing a section through the DAB stained dendrite. The staining was restricted to the injected cell. Boxed area indicates the region examined at higher magnification. Scale bar 2 μm.
(D) High magnification electron micrograph of area in box 2 from (B) showing that antibody associated staining (dark material; see arrow) occurs only in the biocytin filled cell. Scale bar 0.5 μm.

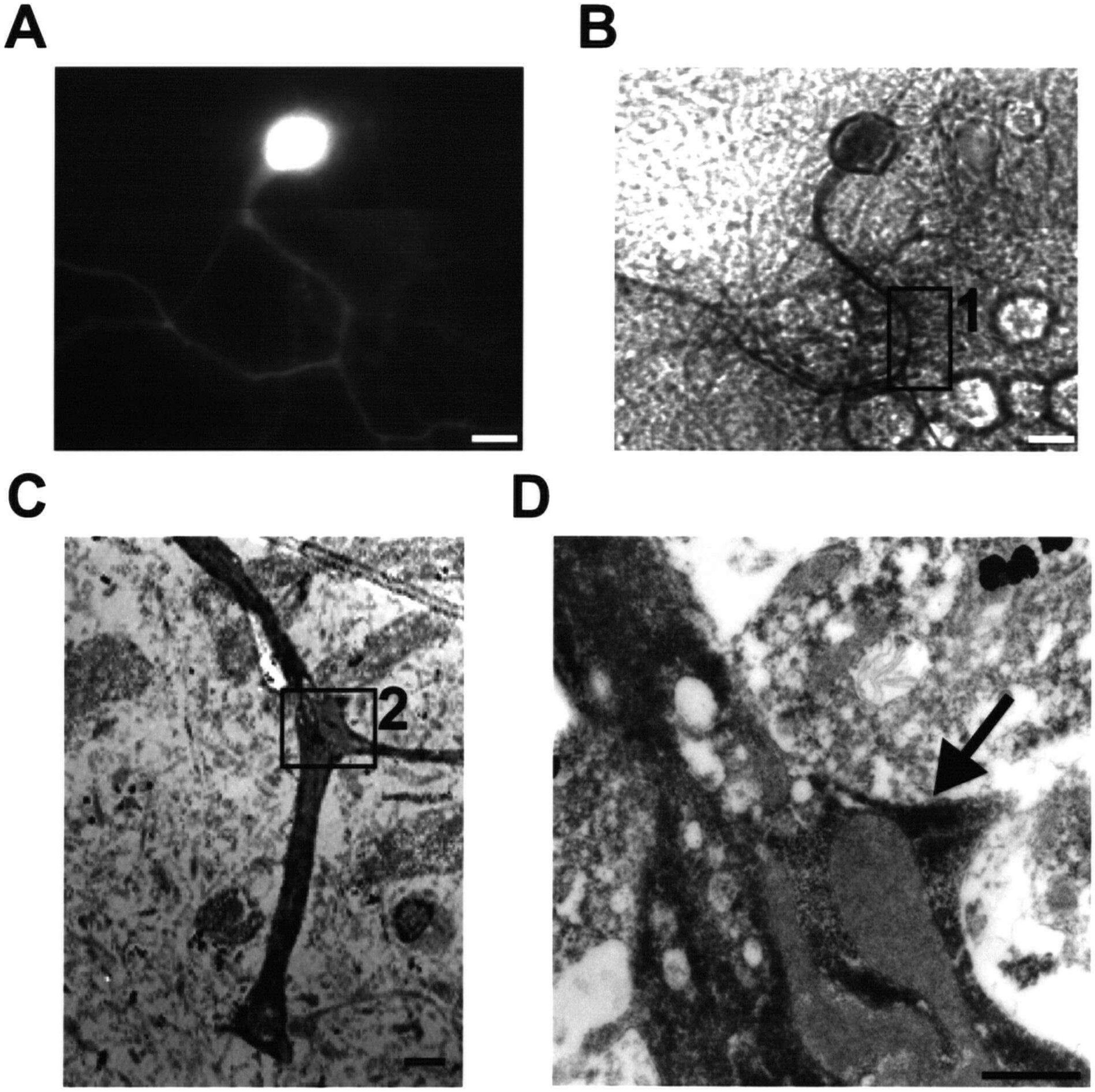
A
B
1
C
2
D

To demonstrate that single cell immunostaining is compatible with imaging of $[Ca^{2+}]_i$ on fine dendritic processes, we have performed the staining procedure on processes that were evaluated using imaging (as described in Murphy et al. 1995). In Figure-8 the hippocampal neuron shown was dialyzed under whole cell voltage mode with a patch pipette solution containing both biocytin and the calcium indicators fluo-3 and mag-fura-2. In these experiments the low affinity Ca^{2+} dye mag-fura-2 (Kd $\approx$ 30 µM; see Raju et al., 1989) is included so that a ratio can be made to correct for process thickness and variation in illumination. Images of mag-fura-2 fluorescence were also used to create a map of the soma and dendrites of the neuron shown (Figure-8A). The boxed area indicates the region imaged (as described above) for miniature $[Ca^{2+}]_i$. In this region several dimly fluorescing spines were seen projecting off the main process. At one of the spines noted #1 (Figure-8C) a miniature calcium transient was observed (Figure-8C & 8D). This transient was confined to within 3 µm of its source at the spine. Immunostaining of this cell with a primary antibody to GluR 2/3, with avidin coupled GO and local production of H_2O_2 revealed selective staining of the main dendrite and a subset of its spines (Figure-8B & 8C). In particular, a spine that was present near the origin of the transient was stained. Following the light microscopic analysis, the cell was processed and the area of interest was examined using electron microscopy (Figure-9). It was revealed that, within the area of interest, the three dimly fluorescing spines corresponded to three distinct GluR 2/3 immunoreactive spines (Figure-9B).

Figure-8. Localization of GluR 2/3 subunits at functionally characterized synapses.

(A) Composite fluorescence mag-fura-2 image of a cultured hippocampal neuron filled with fluo-3, mag-fura-2, and biocytin. Boxed area indicates the region imaged during the experiment. Scale bar 20 μm.
(B) (top) Averaged mag-fura-2 fluorescence image of area of interest captured by a CCD camera. (bottom) Photograph of area of interest DAB stained for GluR 2/3 subunits using the single cell immunostaining procedure. Boxed areas show the area of interest examined at higher magnification in (C). Scale bar 8 μm.
(C) Magnified images of the area of interest. Arrows indicate 3 sites where Ca^{2+} sensitive fluo-3 fluorescence was monitored. These sites appear out of focus since they do not lie within the same focal plane as the main dendritic branch. Spine #1 is indicated on the image of GluR 2/3 staining.
(D) Plots of fluo-3 fluorescence normalized to process volume for 3 indicated dendritic sites. A local Ca^{2+} transient was initiated at site #1 (see arrow).

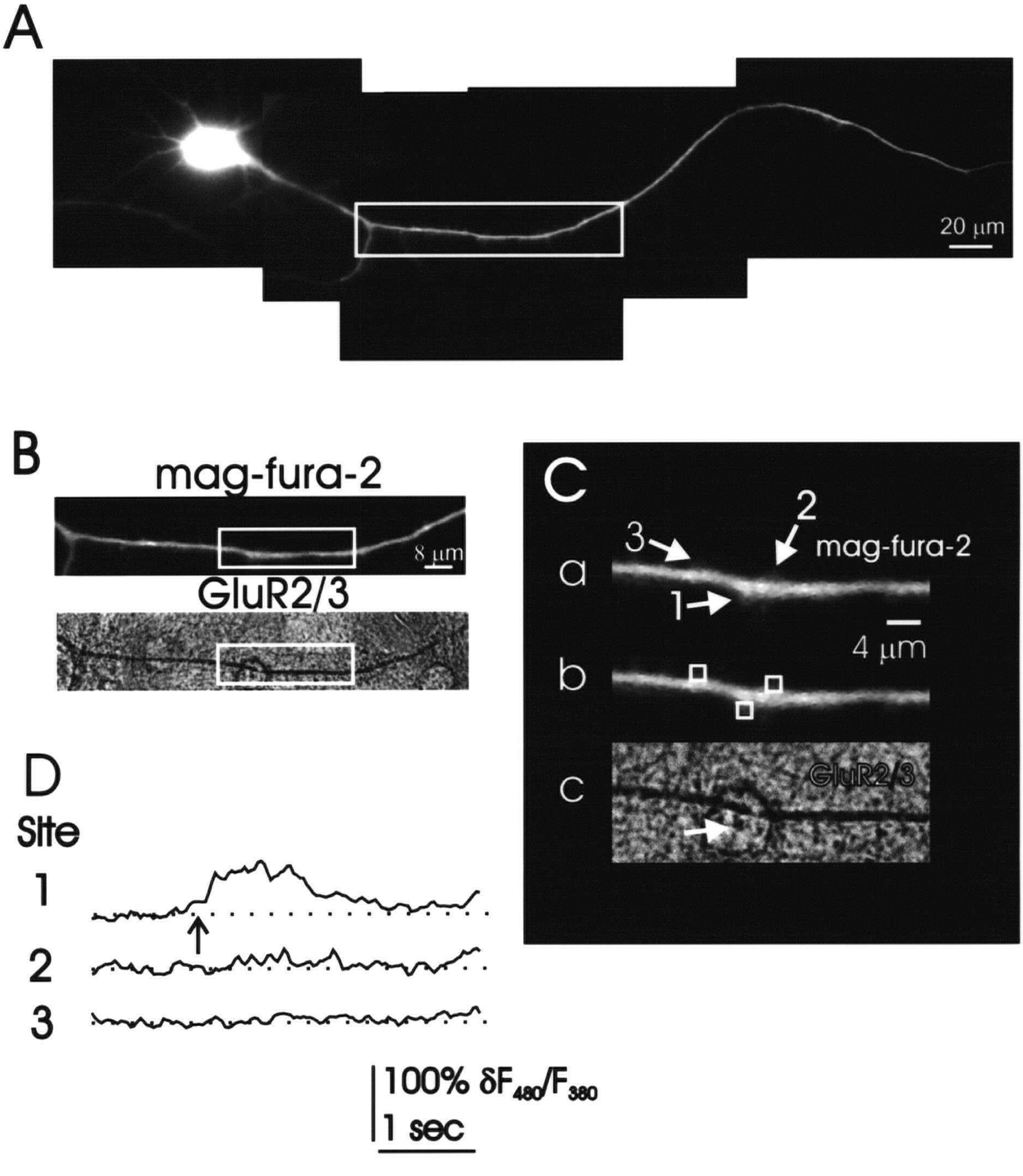
A
20 µm
B
mag-fura-2
8 µm
GluR2/3
C
a
3
2
mag-fura-2
1
4 µm
b
c
GluR2/3
D
Site
1
2
3
100% δF$_{480}$/F$_{380}$
1 sec

4.8 Peroxide clearance of catalase conjugated beads

A potential weakness of the single cell method is the staining of neighboring cells due to diffusion of H_2O_2 out of the cell of interest. This is particularly problematic when staining for antigens that are not present in the cell body such as Tau-1 (an axonal protein), or MAP-2 (a dendritic protein). Due to the comparatively large volume of the cell body, the amount of H_2O_2 generated by GO is highest within the cell body than anywhere else in the cell. If the antigen of interest is absent from the cell body, H_2O_2 produced in the cell body will not be used by peroxidase (conjugated to the secondary antibody) and it will leak out of the cell. This in turn, will result in staining of the processes of the neighboring cells. In an effort to solve this problem, we have successfully conjugated catalase, an enzyme which breaks down H_2O_2, to agarose beads while maintaining some catalase activity (Figure-10). Agarose beads prevent catalase from entering permeabilized cells . Therefore any H_2O_2 present in the extracellular solution will be degraded by catalase, while the H_2O_2 generated inside the cell of interest is not affected. The activity of the conjugated catalase was initially tested by adding the beads to a solution of DAB/H_2O_2 (data not shown). After 3 min. HRP was added to the mixture. The DAB/H_2O_2 solution containing catalase conjugated beads did not change color, whereas the DAB/H_2O_2 solution containing non-conjugated beads formed a dark precipitate. Thus, it was concluded that the conjugated beads were able to break down H_2O_2 during the 3 min. preincubation period. Following this preliminary result, o-dianisidine method of Maehly and Chance (1954) was used to quantitate the activity of the catalase beads. HRP in the presence of peroxide oxidizes o-dianisidine to a product which has an absorbance peak at 450 nm. When HRP and o-dianisidine are present in

Figure-9. Localization of GluR 2/3 subunits at single CNS synapses.

(A) (top) Averaged mag-fura-2 fluorescence image of area of interest (investigated in Figure-6) captured by a CCD camera. Arrows indicate the sites where Ca^{2+}-sensitive fluorescence and miniature synaptic events were monitored. (bottom) Photograph of area of interest DAB stained for GluR 2/3 subunits using single cell method. Site 1 is indicated in this photograph by an arrow. Scale bar 4 μm.
(B) Electron micrographs of the three functionally characterized sites. All three sites correspond morphologically to dendritic spines. The dark precipitates correspond to GluR 2/3 subunits staining which is restricted to the cell of interest. Scale bar 1 μm.
(C) Schematic representation of the three functionally characterized sites showing the structural differences in these sites. The figure was prepared by tracing the outline of each spine from the electron micrographs. Note, the lack of glutaraldehyde fixation and the triton X-100 incubation lead to some degradation of ultrastructure.

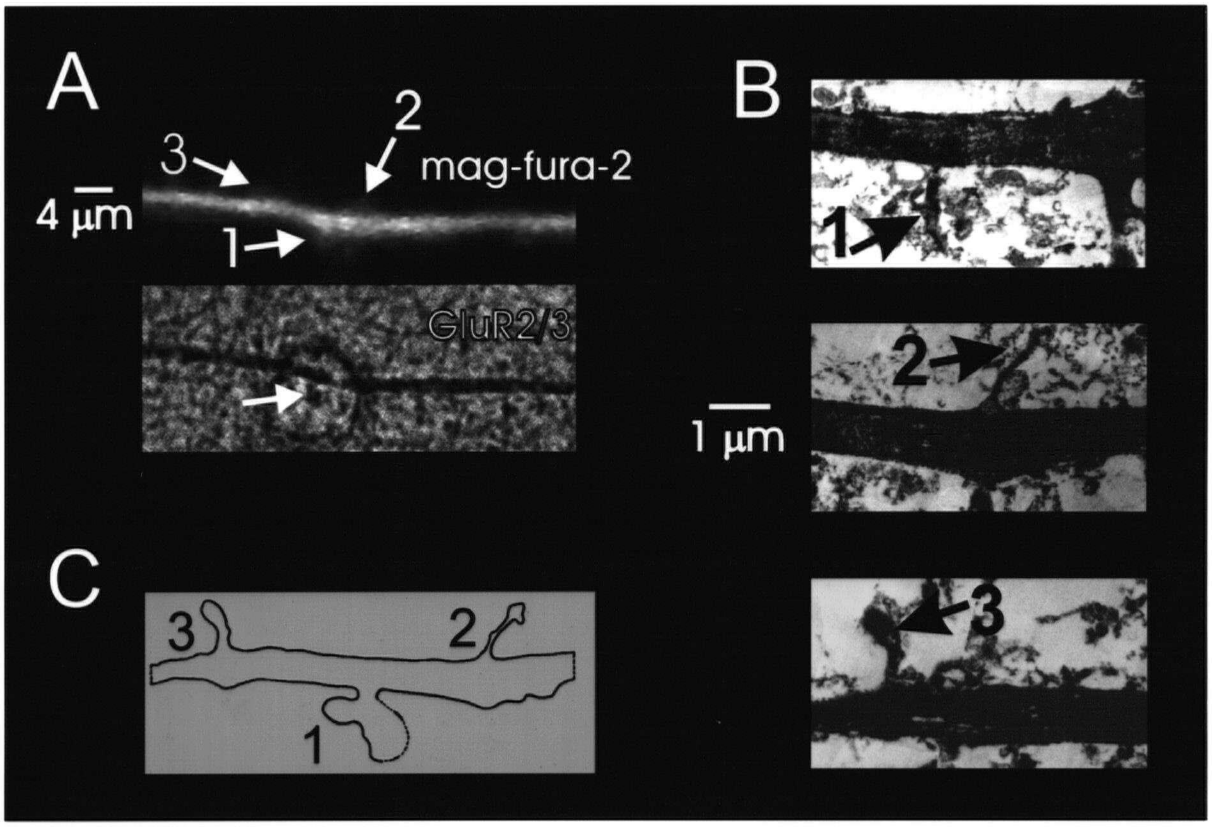
A
2
3
mag-fura-2
4 µm
1
GluR2/3
B
1
2
1 µm
C
3
2
1
3

excess upon addition of the quenching mixture containing peroxide, the absorbance at 450 is reflective of the amount of the peroxide present in the quenching solution. The amount of peroxide, in turn, is dependent on the activity of catalase present in the quenching solution. Thus, if the catalase activity is high, the amount of peroxide in the quenching solution would be low, resulting in low absorbance value upon addition to the substrate solution (Figure-10A). If the catalase activity is low in the quenching solution, the amount of peroxide remains high resulting in a high absorbance value upon addition to the substrate solution. The catalase activity of the beads (both conjugated and unconjugated) was estimated by determining initial slope of their respective absorbance curves, and normalizing the values for the slope of the absorbance curve of the free catalase (Figure-10B). Based on this assay, the conjugated beads have approximately six times the catalase activity of the unconjugated beads. The catalase activity of the unconjugated beads reflects the spontaneous degredation of H_2O_2 in solution. It must be emphasized that this experiment was conducted simply to demonstrate an approach for restricting the generation of peroxide to a cell of interest. For this purpose, the determination of the absolute value of catalase activity of the beads was deemed unnecessary.

Figure-10. Peroxide clearance activity of catalase-conjugated agarose

(A) Plot of absorbance at 450 nm of solution of HRP and o-dianisidine upon addition of a quenching solution at known time intervals. The absorbance at 450 represents the amount of peroxide present in solution at each point in time. The quenching solution consists of a mixture of peroxide with unconjugated beads(●), or catalase-conjugated beads (■), or free catalase (▲).

(B) Normalized catalase activity of unconjugated beads compared to that of the catalase-conjugated beads. The normalized activity was calculated by determining the ratio of the initial slope of the absorbance trace of each bead from (A) to the initial slope of the free catalase trace.

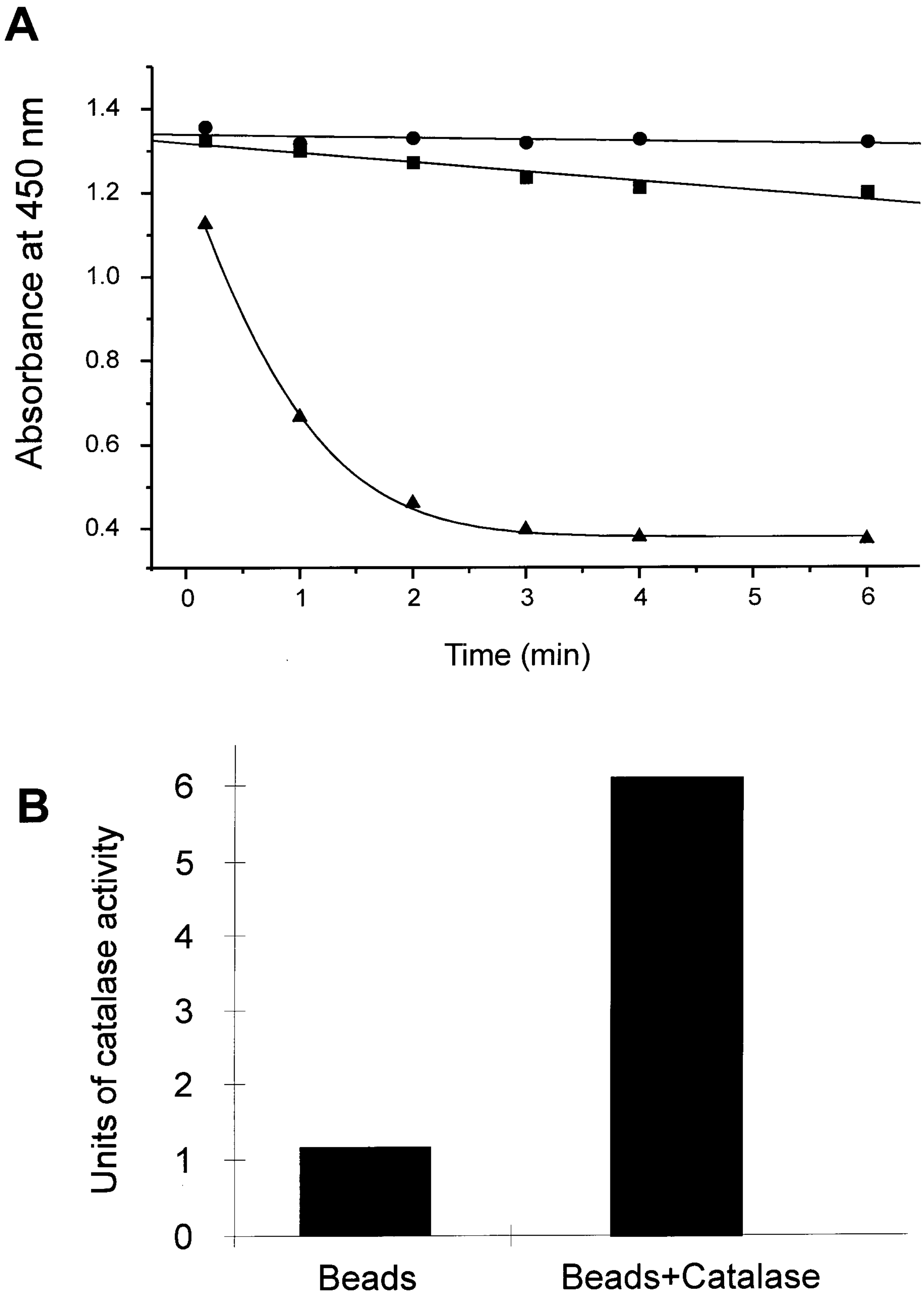
A
Absorbance at 450 nm
1.4
1.2
1.0
0.8
0.6
0.4
0
1
2
3
4
5
6
Time (min)
B
Units of catalase activity
6
5
4
3
2
1
0
Beads
Beads+Catalase

CHAPTER V

Discussion

5.1 A combined method for functional and structural examination of a single synapse

While structural changes have been implicated by many researchers as an important determinant of synaptic strength, to date, no direct evidence exists in support of this hypothesis in mammalian CNS. The main reason for the lack of direct evidence is that the current studies (Schikorski and Stevens, 1997) are based on population data, meaning that the functional properties of a population of synapses were correlated with the structural properties of the population. In order to determine the exact relationship between synaptic strength and synaptic morphology, it is necessary to examine these two properties in the same synapse. We have proposed a simple 3 step method in which we have combined the most widely used methods of structural and functional analysis of single CNS synapses.

In our proposed method, measurement of $[Ca^{2+}]_i$ using optical techniques was used to assess the function of a single synapse. As previously mentioned, in contrast to electrophysiological approaches, optical techniques are easier to perform and they provide a better resolution of postsynaptic events to individual synapses. Wide-field microscopy using a CCD camera was chosen over confocal microscopy to detect the arrival of MSCTs for two reasons. First, quantum efficiency (defined as the proportion of photons arriving at a detector which contribute to the output of the detector; Pawley, 1995) of a PMT (~30%) is lower than the quantum efficiency of a CCD (~50% for our camera). Therefore, when using CLSM a greater number of photons are required to generate a signal than is needed when using a CCD camera, which leads to increased photobleaching and photodynamic damage. Secondly, a CCD camera forms an image by simultaneously recording the information from all points of the object plane. In contrast, a CLSM detects the intensity of each pixel one after another. Hence, the imaging speed of a CLSM is limited by the scanning rate of the microscope (Schild, 1996). The imaging rate of our confocal microscope is approximately 3 frames/sec, compared to 30 frames/sec for our CCD camera. As seen in Figure-2B, the kinetic profile of a MSCT is too fast to be described by our confocal microscope. However, it must be noted that with the line scanning mode, the time resolution of a CLSM can be increased to approximately 1 line/2 msec In this mode, a single line through the object plane is scanned repeatedly (Schild, 1996). The price for the increased rate however, is loss of the 2D resolution.

While a CCD camera provides a fast enough temporal resolution for detecting MSCTs, our CLSM has a higher spatial resolution (both lateral and axial) than our CCD camera (Figure-1). In addition, imaging with a confocal microscope allows for an easy way of estimating the size of large numbers of spines, as well as reconstructing the spines in 3D. Because of these two reasons, CLSM was deemed a useful method of examining the synapse structure. In order to fluorescently label a cell of interest, biocytin was included in the patch solution during $[Ca^{2+}]_i$ imaging. Biocytin is easy to inject, does not damage the injected cell, yields low-resistance recording electrodes, and remains in the cell for a long period of time without leaking (Tasker et al., 1991; Kita and Armstrong, 1991). More importantly, biocytin has high affinity and specificity for avidin, which can be conjugated to various dyes such as fluorescein (Figure-2Ab).

Much of the information regarding the structure of a synapse, such as the size of the presynaptic vesicular pool or the PSD, cannot be attained directly at the level of the light microscope. The last step in our proposed method allows for EM analysis of the cell of interest. This is achieved by DAB (which forms an electron-dense precipitate) mediated staining of avidin immunoreactivity. In this particular experiment, a primary antibody against avidin was used. It must be noted that, since for the purpose of confocal microscopy the cell of interest was labeled with fluorescein-conjugated avidin, using a primary antibody against fluorescein (Vector Laboratories) would have been equally effective in producing EM-detectable DAB staining. Previously, there have been several studies in which confocal microscopy was combined with EM. In these studies, the most common method of combining the two techniques was the photo-oxidation of the fluorescent dye into an electron-dense material (Maranto, 1982). In comparison to our proposed method, photo-oxidation is far more labour intensive as specimens must be processed section by section. More recently, Sun et al. (1998) have reported a rapid method for combined CLSM and EM visualization of biocytin-labeled neurons. In this method, a biocytin-filled neuron is reacted with avidin-fluorescein and imaged with a confocal microscope. To convert the fluorescent label to an EM-detectable signal, the cell is then treated with a biotin/HRP complex and stained with DAB/H_2O_2. Considering that a single avidin molecule has four binding sites for biotin, this method relies on recognition of avidin-fluorescein's excess biotin binding sites by the biotin/HRP complex (Sun et al., 1998). When compared to our proposed method, while our method allows for further amplification of the EM-detectable signal by using an antibody against avidin, the price of this amplification step is the increased risk of non-specific staining associated with the additional antibody (anti-avidin) step.

5.2 Local generation of H_2O_2 by glucose oxidase allows for restriction of antibody staining to a single cell

Despite the recent advances in the field of immunocytochemistry, many questions have still remained unanswered regarding the immunocytochemical makeup of single functionally characterized synapses. The main difficulty lies with restricting the immunocytochemical staining to a neuron of interest (to reduce reactivity of neighboring cells). While the use of low density neuronal cultures has allowed for receptor localization (by immunofluorescence) to individual synapses (Craig et al., 1993; Dong et al., 1997), the application of immunofluorescence to systems of greater complexity such as high density cell cultures or brain slices does not necessarily permit the resolution of fine dendrites attributed to a single neuron. Hence, we have developed a staining technique which allows for examination of the immunocytochemical make-up of functionally characterized synapses of a single neuron in the presence of many neighbors. This method, in principle, is based on the commonly used immunoperoxidase technique developed by Avrameas and Uriel (1966). In our modified approach, the staining is restricted to a single cell by localizing the generation of H_2O_2 (a substrate for the immunoperoxidase reaction) to the cell of interest. This is achieved by selectively loading the cell of interest with GO using the avidin-biocytin linkage (Figure-3). GO (β-D-glucose: oxygen 1-oxoreductase, EC 1.1.3.4) is a 131 KDa protein which oxidizes β-D-glucose to gluconolactone accompanied by the production of H_2O_2 (Frederick et al., 1990). Conveniently, GO is already available commercially in a form conjugated to avidin for use in immunocytochemical protocols in which GO oxidation of tetrazolium salts is used as a stain. We have exploited the ability of Av-GO to generate H_2O_2 to confine antibody-mediated staining to a single cell.

5.3 Penetration properties of avidin compared to that of avidin conjugated to glucose oxidase

The underlying basis of our technique requires that GO (as part of the Av-GO complex) be distributed uniformly throughout the cell of interest. One of the factors influencing the distribution of Av-GO is the rate of diffusion of Av-Go into permeabilized cells. A time course of GO diffusion was obtained empirically in order to determine the minimum incubation period for Av-GO (data not shown). Based on our results, the minimum incubation time for unconjugated avidin was only one hour, while Av-GO (at the same concentration) required approximately 12 hours to completely diffuse into cells. This difference is most likely due to the fact that avidin is a much smaller protein (67 KDa; Gope et al., 1987) than Av-GO (>197 KDa).

5.4 Glutaraldehyde prevents the penetration of avidin conjugated to glucose oxidase into cells

An important factor influencing the distribution of GO within a cell is the fixation procedure. Numerous fixation protocols exist (for a review see Hopwood, 1985) each with varying efficacy with regards to preservation of morphology and antigenicity. In our experiments, we examined the effects of three commonly used fixation protocols on Av-GO penetration (a necessary component of our staining procedure) into cells. Based on our results, para-formaldehyde or formalin fixation does not hinder the penetration of Av-GO (Figure-4). In contrast, glutaraldehyde blocks the diffusion of Av-Go into the cell body as well as the processes. Marked reduction in tissue permeability with glutaraldehyde fixation is likely due to extensive cross-linking of cellular proteins (Hopwood, 1985). For the same reason, glutaraldehyde has become the fixative of choice for ultrastructural analysis since it provides excellent morphological preservation (Hopwood, 1985). Since the main incentive for developing the single cell staining technique was to determine the immunocytochemical structure of single CNS synapses, we have modified our protocol to still allow for ultrastructural analysis. Hence, in the proposed single cell staining protocol, cells are initially fixed with para-formaldehyde, and subsequent to immunostaining, cells are post-fixed with glutaraldehyde to allow for ultrastructural examination using EM. With glutaraldehyde postfixation, it is likely that some degradation of ultrastructure occurs. However, given the large number of fixation protocols (Hopwood, 1985), we anticipate that fixation may be optimized.

5.5 Distribution of NSE within a single cortical neuron

The specificity of our single cell staining method at the light microscopic level was demonstrated by immunostaining a single neuron for NSE. The observed cytoplasmic staining within the soma, and the proximal as well as distal processes (Figure-4B) is consistent with previous studies in which NSE within rat primary cortical cultures was localized by means of conventional immunocytochemistry (Secchi et al., 1980). Furthermore, single cell NSE staining revealed the presence of NSE within dendritic spines at the light microscopic level (not previously reported). A potential concern with the single cell method was the possibility of H_2O_2 leakage from the cell of interest to neighboring cells resulting in non-specific staining. Our single cell NSE staining revealed that despite the cell of interest being enveloped with NSE-immunoreactive processes of neighboring cells, the peroxidase antibody-mediated staining was restricted to the cell of interest (Figure-4B & 4C). It must be emphasized that while leakage of H_2O_2 could result in staining of neighboring cells, this staining would be expected to be specific for the antigen of interest as it is dependent on the presence of a primary antibody. Hence, even in the event of leakage of H_2O_2, single cell staining would still accurately localize the antigen within a cell of interest.

5.6 Specificity of single cell method at the ultrastructural level as revealed by GluR 2/3 staining

Electron microscopic examination of GluR 2/3 single cell staining provided evidence for cell specificity of our method at ultrastructural level (Figure-5). In addition, it was shown that glutaraldehyde post-fixation is compatible with single cell staining procedure (albeit ultrastructure preservation could be improved). Thus, using this approach, single cell staining allows for investigation of the immunocytochemical make-up of single synapses using both light and electron microscopy. The observed light microscopic localization of GluR 2/3 (Figure-5B) is consistent with the previous report of glutamate receptor distribution in cultured hippocampal neurons (Craig et al., 1993). In agreement with this study (in which the same antibody as ours was used), GluR 2/3 immunoreactivity was found in the neuronal somata, dendritic shafts, and dendritic spines. Although the possibility of artifactual spread of DAB precipitate cannot be completely ruled out, the abundance of DAB staining throughout the cytosol may reflect the synthesis, modification, assembly and transport of glutamate receptors in the cytoplasm (Ginsberg et al., 1995; Tachibana et al., 1994; Petralia et al., 1994; and Craig et al., 1993). It is worth noting that in their study, in which 1-3 weeks old cultured hippocampal neurons were examined, Craig et al. (1993) suggested that clustering of the glutamate receptors within the postsynaptic membrane may occur in later stages of the development. Furthermore, they observed complete colocalization of GluR 1 and GluR 2/3 subunits in cultured hippocampal neurons (ibid.).

5.7 Localization of AMPA-type glutamate receptors at functionally characterized synapses

We anticipate that our single cell immunostaining procedure will have greatest utility when compared with cellular physiological and imaging studies. For example, we have demonstrated a combined functional and light/ultrastructural examination of three individual synapses within a single cortical neuron. The activity of these synapses were mapped using Ca^{2+} imaging (Figure-6) and subsequently using single cell method the synapses were shown to contain GluR 2/3 subunits (Figure-7). Interestingly, most dendritic regions showed staining for the AMPA-type glutamate receptor GluR 2, suggesting that regulation of AMPA mediated synaptic potentials during plasticity may involve regulation of existing receptors (Isaac et al., 1995; Liao et al., 1995; Wang et al., 1996).

5.8 Future considerations for the application of single-cell staining

In addition to the above experiments, using single cell staining we have successfully localized various other intracellular antigens including MAP-2 and β-tubulin within a single neuron (data not shown). In principle, the single cell method should also allow for localization of extracellular antigens (albeit single cell specificity may not be as good as it is for intracellular antigens). By conjugating catalase to agarose beads we have demonstrated a way to prevent non-specific staining of neighboring cells due to the escape of H_2O_2 out of the cell of interest (Figure-10). This allows for the single-cell method to be used for localizing extrasomatic antigens. In addition, we are currently optimizing our method for use in more complex cellular systems such as brain slices.

As previously mentioned, the structural relationships of synapses in 3D gives insight to the functional role of synapses. Since confocal microscopy is by far the easiest technique for examining biological structures in 3D, we have conducted preliminary experiments to produce a fluorescent signal using the single-cell method. In these experiments the single cell staining method was conducted as described previously with one exception: the final DAB/glucose staining solution was replaced by a fluorescein-tyramide/glucose solution (Mandel Scientific, Guelph, ON). Fluorescein-tyramide acts as a substrate for HRP. As originally described by Bobrow et al. (1989), HRP in the presence of H_2O_2 catalyses the deposition of tyramide onto the enzyme surface. Tyramide can be commercially obtained with various fluorophore conjugates such as fluorescein-tyramide and Texas Red-tyramide (for a review see Kricka, 1993).

5.9 Conclusions

By means of $[Ca^{2+}]_i$ imaging, the activity of 4 synapses belonging to a cultured rat cortical neuron was assessed. In addition, using confocal microscopy, the size of the postsynaptic spines of the characterized synapses was compared. Subsequently, the neuron of interest was labeled with an electron-dense material (DAB) for EM analysis. With this approach we have demonstrated a way in which the function of a single synapse can be correlated to its structure both at light and EM levels. We believe that this type of analysis is the key to determining the exact role of structural modifications in the establishment and the maintenance of neuronal plasticity.

Furthermore, using our single cell staining technique, we successfully localized AMPA-type glutamate receptor GluR-2 in a single cultured cortical neuron, as well as in functionally characterized synapses of a hippocampal neuron. The presence of GluR-2 in most dendritic regions of the examined hippocampal neuron suggests that the regulation of AMPA-mediated synaptic potentials during plasticity may involve regulation of existing receptors (silent receptor hypothesis; Isaac et al., 1995; Liao et al., 1995; Wang et al., 1996). While more extensive study of this correlation lies beyond the scope of our discussion, the employed experimental approach introduces a powerful tool for answering many of the questions regarding the regulation of synaptic transmission. In addition, it is hoped that single cell staining will facilitate the identification of the receptor composition of synapses of neurons, in complex preparations such as brain slices.

Literature Cited

Alford S., Frenguelli B. G., Schofield J. G., and Collingridge G. L. (1993) Characterization of Ca^{2+} signals induced in hippocampal CA1 neurones by the synaptic activation of NMDA receptors. *J. Physiol.* **469:** 693-716.

Amaral D. G., Ishizuka N., and Claiborne B. (1990) Neurons, numbers and the hippocampal network. *Prog. Brain Res.* **83,** 1-11.

Avrameas S., and Uriel J. (1966) [Method of antigen and antibody labeling with enzymes and its immunodiffusion application]. [French] *Comptes Rendus Hebdomadaires des Seances de l Academie des Sciences - D: Sciences Naturelles* **262,** 2543-5.

Bailey C. H., and Kandel E. R. (1993) Structural changes accompanying memory storage. *Annu. Rev. Physiol.* **55:** 397-426.

Bannister N. J., and Larkman A. U. (1995) Dendritic morphology of CA1 pyramidal neurones from the rat hippocampus: II. Spine distributions. *J. Comp. Neurol.* **360:** 161-71.

Bear M. F., and Malenka R. C. (1994) Synaptic plasticity: LTP and LTD. *Current Opinion in Neurobiology.* **4:** 389-99.

Betz W. J., Mao F., and Bewick G. S. (1992) Activity-dependent fluorescent staining and destaining of living vertebrate motor nerve terminals. *J. Neurosci.* **12:** 363-75.

Bliss T. V., and Collingridge G. L. (1993) A synaptic model of memory: long-term potentiation in the hippocampus. *Nature.* **361:** 31-9.

Bliss T. V., and Lomo T. (1973) Long-lasting potentiation of synaptic transmission in the dentate area of the anaesthetized rabbit following stimulation of the perforant path. *J. Physiol.* **232:** 331-56.

Bobrow M. N., Harris T. D., Shaughnessy K. J., and Litt G. J. (1989) Catalyzed reporter deposition, a novel method of signal amplification. Application to immunoassays. *J. Imm. Meth.* **125:** 279-85.

Cole K. S., (1949) Dynamic electrical characteristics of the squid axon membrane. *Arch. Sci. Physiol.* **3:** 253-258.

Collingridge G. L., and Bliss T. V. (1995) Memories of NMDA receptors and LTP. *Trends Neurosci.* **18:** 54-6.

Craig A. M., Blackstone C.D., Huganir R.L., and Banker G. (1993) The distribution of glutamate receptors in cultured rat hippocampal neurons: postsynaptic clustering of AMPA-selective subunits. *Neuron* **10,** 1055-68.

Cuello, A. C. (1993) In: Immunohistochemistry II. (Smith, D.A., ed) John Wiley & Sons Ltd.

Denk W., Yuste R., Svoboda K., and Tank D. W. (1996) Imaging calcium dynamics in dendritic spines. *Current Opinion in Neurobiology.* **6:** 372-8.

Desmond N. L., and Levy W. B. (1988) Synaptic interface surface area increases with long-term potentiation in the hippocampal dentate gyrus. *Brain Res.* **453:** 308-14.

Dong H., O'Brien R. J., Fung E. T., Lanahan A. A., Worley P. F., and Huganir R. L. (1997) GRIP: a synaptic PDZ domain-containing protein that interacts with AMPA receptors. *Nature* **386,** 279-84.

Eccles J. C. (1965) Possible ways in which synaptic mechanisms participate in learning, remembering and forgetting. In: The Anatomy of Memory (Kimble DP, ed), pp 97. Palo Alto: Science and Behavior Books.

Fonseca M. I., and Brown R. D. (1997) Immunocytochemical methods for investigating receptor localization. *Meth. Mol. Biol.* **83,** :91-106.

Forti L., Bossi M., Bergamaschi A., Villa A., and Malgaroli A. (1997) Loose-patch recordings of single quanta at individual hippocampal synapses. *Nature.* **388:** 874-8.

Frederick K. R., Tung J., Emerick R. S., Masiarz F. R., Chamberlain S. H., Vasavada A., Rosenberg S., Chakraborty S., Schopfer L. M., Schopfer L. M. and Massey V. (1990) Glucose oxidase from Aspergillus niger. Cloning, gene sequence, secretion from Saccharomyces cerevisiae and kinetic analysis of a yeast-derived. *J. Biol. Chem.* **265,** 3793-802.

Frey U., and Morris R. G. (1997) Synaptic tagging and long-term potentiation. *Nature* **385,** 533-6.

Ginsberg S. D., Price D. L., Blackstone C. D., Huganir R. L., and Martin L. J. (1995) The AMPA glutamate receptor GluR3 is enriched in oxytocinergic magnocellular neurons and is localized at synapses. *Neurosci.* **65:** 563-75.

Globus A. (1975) Brain morphology as a function of presynaptic morphology and activity. In: The developmental neuropsychology of sensory deprivation (Reisen AH, ed), pp 9-91. New York: Academic.

Gope M. L., Keinanen R. A., Kristo P. A., Conneely O. M., Beattie W. G., Zarucki-Schulz T., O'Malley B. W., and Kulomaa M. S. (1987) Molecular cloning of the chicken avidin cDNA. *Nucleic Acids Research.* **15:** 3595-606,.

Greenough W. T., and Bailey C. H. (1988) The anatomy of a memory: convergence of results across a diversity of tests. *Trends Neurosci.* **11:** 142-147.

Hamill O. P., and Sakmann B. (1981) Multiple conductance states of single acetylcholine receptor channels in embryonic muscle cells. *Nature.* **294:** 462-4.

Harris K. M., and Kater S. B. (1994) Dendritic spines: cellular specializations imparting both stability and flexibility to synaptic function. *Ann. Rev. Neurosci.* **17:** 341-71.

Harris K. M., and Sultan P. (1995) Variation in the number, location and size of synaptic vesicles provides an anatomical basis for the nonuniform probability of release at hippocampal CA1 synapses. *Neuropharm.* **34:** 1387-95.

Harris K. M., and Stevens J. K. (1989) Dendritic spines of CA 1 pyramidal cells in the rat hippocampus: serial electron microscopy with reference to their biophysical characteristics. *J. Neurosci.* **9:** 2982-97.

Hebb D. O. (1949) In: The organization of behavior. New York: Wiley.

Hodgkin A. L., Huxley A. F., and Katz B. (1949) Ionic currents underlying activity in the giant axon of the squid. *Arch. Sci. Physiol.* **3:** 129-150.

Hollmann M., and Heinemann S. (1994) Cloned glutamate receptors. *Ann. Rev. Neurosci.* **17,** 31-108.

Hopwood D. (1985) Cell and tissue fixation, 1972-1982. *Histoche. J.* **17,**:389-442.

Horner C. H. (1993) Plasticity of the dendritic spine. *Prog. Neurobio.* **41:** 281-321.

Hosokawa T., Rusakov D. A., Bliss T. V., and Fine A. (1995) Repeated confocal imaging of individual dendritic spines in the living hippocampal slice: evidence for changes in length and orientation associated with chemically induced LTP. *J. Neurosci.* **15:** 5560-73.

Huntley G. W., Vickers J. C., and Morrison J. H. (1994) Cellular and synaptic localization of NMDA and non-NMDA receptor subunits in neocortex: organizational features related to cortical circuitry, function and disease. *Trends Neurosci.* **17:** 536-43.

Inoué S. (ed.) (1986) In: Video Microscopy, pp. 197-203. New York; Plenum.

Isaac J. T., Nicoll R. A., and Malenka R. C. (1995) Evidence for silent synapses: implications for the expression of LTP. *Neuron* **15,** 427-34.

Jaffe D. B., Fisher S. A., and Brown T. H. (1994) Confocal laser scanning microscopy reveals voltage-gated calcium signals within hippocampal dendritic spines. *J. Neurobio.* **25:** 220-33.

Kita H., and Armstrong W. (1991) A biotin-containing compound N-(2-aminoethyl)biotinamide for intracellular labeling and neuronal tracing studies: comparison with biocytin. *J. Neurosci. Meth.* **37:** 141-50.

Kricka L. J. (1993) Ultrasensitive immunoassay techniques. *Clin. Bioch.* **26:** 325-31.

Kullmann D. M., and Siegelbaum S. A. (1995) The site of expression of NMDA receptor-dependent LTP: new fuel for an old fire. *Neuron.* **15:** 997-1002.

Liao D., Hessler N. A., and Malinow R. (1995) Activation of postsynaptically silent synapses during pairing-induced LTP in CA1 region of hippocampal slice. *Nature* **375,** 400-4.

Lisman J. (1989) A mechanism for the Hebb and the anti-Hebb processes underlying learning and memory. *Proc. Natl. Acad. Sci. U.S.A.* **86:** 9574-8.

Liu G., and Tsien R. W. (1995) Synaptic transmission at single visualized hippocampal boutons.
Neuropharm. **34:** 1407-21.

Maehy A. C., and Chance B. (1954) *Methods Biochem. Anal.* **1:** 357-424.

Malinow R., Otmakhov N., Blum K. I., and Lisman J. (1994) Visualizing hippocampal synaptic function by optical detection of Ca2+ entry through the N-methyl-D-aspartate channel. *Proc. Natl. Acad. Sci. U.S.A.* **91,** 8170-4.

Maranto A. R. (1982) Neuronal mapping: a photooxidation reaction makes Lucifer yellow useful for electron microscopy. *Science.* **217:** 953-5.

Marmont G. (1949) Studied on the axon membrane. I. A new method. *J. Cell. Comp. Physiol.* **34:** 351-382.

Miles R., Toth K., Gulyas A. I., Hajos N., and Freund T. F. (1996) Differences between somatic and dendritic inhibition in the hippocampus. *Neuron.* 16: 815-23.

Moser M. B., Trommald M., and Andersen P. (1994) An increase in dendritic spine density on hippocampal CA1 pyramidal cells following spatial learning in adult rats suggests the formation of new synapses. *Proc. Natl. Acad. Sci. U.S.A.* **91:** 12673-5.

Murphy T. H., and Baraban J. M. (1990) Glutamate toxicity in immature cortical neurons precedes development of glutamate receptor currents. *Dev. Brain. Res.* **57,** 146-150.

Murphy T. H., Baraban J. M., Wier W. G., and Blatter L. A. (1994) Visualization of quantal synaptic transmission by dendritic calcium imaging. *Science.* **263:** 529-32.

Murphy T. H., Baraban J. M., and Wier W. G. (1995) Mapping miniature synaptic currents to single synapses using calcium imaging reveals heterogeneity in postsynaptic output. *Neuron.* **15:** 159-68.

Murthy V. N., Sejnowski T. J., and Stevens C. F. (1997) Heterogeneous release properties of visualized individual hippocampal synapses. *Neuron.* **18:** 599-612.

Nairn R. C. (1976) In: Fluorescent Protein Tracing. Edinburgh: Churchill Livingstone.

Pawley, J.B. (ed) (1995) In: Handbook of Biological Confocal Microscopy. New York: Plenum.

Petralia R. S., Wang Y. X., and Wenthold R. J. (1994) Histological and ultrastructural localization of the kainate receptor subunits, KA2 and GluR6/7, in the rat nervous system using selective antipeptide antibodies. *J. Comp. Neurol.* **349:** 85-110.

Raju B. Murphy E. Levy LA. Hall RD. London RE. (1989) A fluorescent indicator for measuring cytosolic free magnesium. *Am. J. Physiol.* **256:** C540-8.

Ramon y Cajal S. (1911) In: Histologie du systeme nerveux de l'homme et des vertebres, Vol II. Paris: Maloine.

Raymond L. A., Blackstone C. D., and Huganir R. L. (1993) Phosphorylation of amino acid neurotransmitter receptors in synaptic plasticity. *Trends Neurosci.* **16:** 147-53.

Regehr W. G., and Atluri P. P. (1995) Calcium transients in cerebellar granule cell presynaptic terminals. *Biophysical Journal.* **68,** 2156-70.

Reynolds, E. S. (1963) The use of lead citrate at high pH as an electron opaque stain in electron microscopy. *J. Cell Biol.* **17,** 208-212.

Ryan T. A., Ziv N. E., and Smith S. J. (1996) Potentiation of evoked vesicle turnover at individually resolved synaptic boutons. *Neuron.* **17:** 125-34.

Sakmann, B., and Neher, E. (eds.). (1983) In: Single Channel Recording. New York: Plenum.

Schikorski T., and Stevens C. F. (1997) Quantitative ultrastructural analysis of hippocampal excitatory synapses. *J. Neurosci.* **17:** 5858-67.

Schild D. (1996) Laser scanning microscopy and calcium imaging. *Cell Calcium.* **19:** 281-96.

Secchi J., Lecaque D., Cousin M. A., Lando D., Legault-Demare L., and Raynaud J. P. (1980) Detection and localization of 14-3-2 protein in primary cultures of embryonic rat brain. *Brain Res.* **184,** 455-66.

Sheng M. (1996) PDZs and receptor/channel clustering: rounding up the latest suspects. *Neuron* **17,** 575-8.

Sorra K. E., and Harris K. M. (1993) Occurrence and three-dimensional structure of multiple synapses between individual radiatum axons and their target pyramidal cells in hippocampal area CA1. *J. Neurosci.* **13:** 3736-48.

Stevens C. F. (1996) Strengths and weaknesses in memory. *Nature* **381:** 471-2.

Stevens C. F., and Sullivan J. (1998) Synaptic Plasticity. *Current Biology* **8:** 151-3.

Sun X. J., Tolbert L. P., Hildebrand J. G., and Meinertzhagen I. A. (1998) A rapid method for combined laser scanning confocal microscopic and electron microscopic visualization of biocytin or neurobiotin-labeled neurons. *J. Hist. & Cyt.* **46:** 263-73,.

Svoboda K. (1998) Shining light on spiny matters. *Nature Neuroscience.* **1:** 93-94.

Tachibana M., Wenthold R. J., Morioka H., and Petralia R. S. (1994) Light and electron microscopic immunocytochemical localization of AMPA-selective glutamate receptors in the rat spinal cord. *J. Comp. Neurol.* **344:** 431-54.

Tasker J. G., Hoffman N. W., and Dudek F. E. (1991) Comparison of three intracellular markers for combined electrophysiological, morphological and immunohistochemical analyses. *J. Neurosci. Meth.* **38:** 129-43.

Taylor D. L., Waggoner A. S., Murphy R. F., Lanni F., and Birge R. R. (eds.) (1986) In: Applications of Fluorescence in the Biomedical Sciences, pp. 3-28. New York: Liss.

Trapp B. D., Marangos P. J., and Webster H.D. (1981) Immunocytochemical localization and developmental profile of neuron specific enolase (NSE) and non-neuronal enolase (NNE) in aggregating cell cultures of fetal rat brain. *Brain Res.* **220,** 121-30.

Tsien R. Y. (1989) Fluorescent probes of cell signaling. *Ann. Rev. Neurosci.* **12:** 227-53.

Tsien R. Y. (1980) New calcium indicators and buffers with high selectivity against magnesium and protons: design, synthesis, and properties of prototype structures. *Biochemistry.* **19:** 2396-404.

Wallace C., Hawrylak, N., and Greenough, W.T. (1991) In: Long Term Potentiation: A Debate of Current Issues (Baudry, M., and Davis, J.L., eds), pp 189: MIT press.

Wang S., Wojtowicz J. M., and Atwood H. L. (1996) Synaptic recruitment during long-term potentiation at synapses of the medial perforant pathway in the dentate gyrus of the rat brain. *Synapse*. **22,** 78-86.

Wojtowicz J. M., Marin L., and Atwood H. L. (1994) Activity-induced changes in synaptic release sites at the crayfish neuromuscular junction. *J. Neurosci.* **14:** 3688-703.

Yuste R., and Denk W. (1995) Dendritic spines as basic functional units of neuronal integration. *Nature.* **375:** 682-4.

Vinores S. A., Herman M. M., Rubinstein L. J., and Marangos P. J. (1984) Electron microscopic localization of neuron-specific enolase in rat and mouse brain. *J. Histochem. & Cytochem.* **32,** 1295-302.